Journal of Computational Physics 230 (2011) 8427–8451

Contents lists available at SciVerse ScienceDirect

Journal of Computational Physics

journal homepage: www.elsevier.com/locate/jcp

Weighted Flow Algorithms (WFA) for stochastic particle coagulation

R.E.L. DeVille [a], N. Riemer [b], M. West [c,*]

[a] Department of Mathematics, University of Illinois at Urbana-Champaign, 1409 W. Green Street, Urbana, IL 61801, USA
[b] Department of Atmospheric Science, University of Illinois at Urbana-Champaign, 105 S. Gregory Street, Urbana, IL 61801, USA
[c] Department of Mechanical Science and Engineering, University of Illinois at Urbana-Champaign, 1206 W. Green Street, Urbana, IL 61801, USA

ARTICLE INFO

Article history:
Received 26 November 2010
Received in revised form 27 June 2011
Accepted 29 July 2011
Available online 10 August 2011

Keywords:
Aerosol modeling
Stochastic simulations
Particle methods
Smoluchowski equations
Multiscale numerics

ABSTRACT

Stochastic particle-resolved methods are a useful way to compute the time evolution of the multi-dimensional size distribution of atmospheric aerosol particles. An effective approach to improve the efficiency of such models is the use of weighted computational particles. Here we introduce particle weighting functions that are power laws in particle size to the recently-developed particle-resolved model PartMC-MOSAIC and present the mathematical formalism of these Weighted Flow Algorithms (WFA) for particle coagulation and growth. We apply this to an urban plume scenario that simulates a particle population undergoing emission of different particle types, dilution, coagulation and aerosol chemistry along a Lagrangian trajectory. We quantify the performance of the Weighted Flow Algorithm for number and mass-based quantities of relevance for atmospheric sciences applications.

1. Introduction

Atmospheric aerosol particles consist of a complex mixture of different chemical species [1] (current models typically contain on the order of 20 different species [2]), with particle diameters ranging from a few nanometers to tens of micrometers. To deal with such high-dimensional and multi-scale data, existing models of atmospheric aerosols on the regional or global scale make large approximations. These generally consist of assuming that all particles within a spatial grid-cell have a composition that depends only on diameter or a few other simple parameters as it is done in sectional aerosol models [e.g. 2–6] or modal aerosol models [e.g. 7–10]. While this makes computation much cheaper, it introduces errors, since it artificially averages the composition of individual particles over a certain size range. These errors are not well-quantified, but could be significant for estimating the effect of aerosols on climate [11].

Recently, particle-resolved aerosol models have been introduced as a way to avoid making *a priori* assumptions about the evolution of particle composition and to more precisely model aerosol microphysics [12–14]. These stochastic models simulate a representative group of particles distributed in composition space, treating coagulation, condensation/evaporation, and other important processes on an individual particle level. Applying such a Monte Carlo approach for simulating the evolution of particle distributions dates back to Gillespie [15], who developed the exact Stochastic Simulation Algorithm [see also 16–18] to treat the stochastic collision-coalescence process in clouds. While the particle-based models are a step forward in accurately representing the detailed interactions which take place amongst aerosol particles, they can be very expensive to run, and are currently not appropriate for simulating aerosol dynamics and chemistry on meso-or macro-scales.

* Corresponding author.
E-mail addresses: rdeville@illinois.edu (R.E.L. DeVille), nriemer@illinois.edu (N. Riemer), mwest@illinois.edu (M. West).
URLs: http://www.math.uiuc.edu/~rdeville/ (R.E.L. DeVille), http://www.atmos.uiuc.edu/~nriemer/ (N. Riemer), http://lagrange.mechse.illinois.edu/mwest/ (M. West).

0021-9991/$ - see front matter © 2011 Elsevier Inc. All rights reserved.
doi:10.1016/j.jcp.2011.07.027

The main thrust of this paper is to introduce an alternate simulation scheme, which reduces the total error for a given cost. To this end, it is useful to consider the types of error inherent in these simulations. There are three distinct sources of error: a finite-number error, a finite-ensemble error, and a time-discretization error. Since computational power is finite, any individual simulation can only treat a finite number of particles, and any aggregate simulation can consider only a finite ensemble of such individual simulations. Moreover, due to the very short timescales in the problem, performing a direct stochastic simulation is too expensive, and one needs to introduce a discrete timestep. We show below that the most significant error in the parameter regimes we consider is—by far—the finite-ensemble error (see, e.g., Figs. 2 and 4). Since the error due to the finiteness of the ensemble is, at its root, a statistical error, the ensemble variance quantifies this error.

The finite-ensemble error is dominant because there are aerosol particles which are comparatively rare yet nonetheless important to the evolution of the aerosol population. Since these particles are rare, a small ensemble size leads to significant sampling errors in these subpopulations; since they are important to the dynamics, these sampling errors percolate throughout the entire population. More concretely, due to the shape of ambient aerosol size distributions and the subsequent evolution, the number of particles in the sub-micron size range is usually several orders of magnitude larger than the particles in the super-micron size range. Both sub-populations are important since the small particles dominate particle number concentration whereas the large particles dominate particle mass concentrations. Moreover, the most likely coagulation events involve interactions of small and large particles. Thus either the population of large particles is under-resolved and the accuracy of the simulation is significantly compromised, or the total number of computational particles in the entire simulation must be immense.

Our way forward is to add the abstraction that a single computational particle can correspond to some number of real particles, i.e. that each computational particle is "weighted" by an appropriate factor. There is a wide variety of choices to be made here: e.g., how one chooses the weighting, the details of how to implement the effect of this weighting, etc. Our approach is to think of each computational particle as corresponding to some number of real particles, and instead of performing some action on a real particle, we perform the action on the computational particle with some probability; this probability scales inversely to the weight. Thus the algorithm can be thought of as a stochastic splitting scheme, where one first determines the type of event as would be done in a direct simulation, and then one decides whether we perform the event on the computational particle. For example, if we have a particle of weight 10^3 in our population, and a direct simulation would call for this particle to be removed, then we remove it with probability 10^{-3}.

Since our simulations involve coagulation events, many events correspond to "triplets" of computational particles (the two particles before the coagulation and the one after). Thus there are many choices for how a stochastic algorithm will treat this triplet, as it could deal with each particle independently, or do so with some correlations. We analyze the most general possible form of such algorithms and optimize over different possible choices. In particular, the particle weighting method that we develop here has smoothly varying particle weights (rather than binning particles into groups with the same weight) and is a function of particle composition (rather than having weights attached to particles [19]). More specifically, the latter means that the weight of a given particle can change during the course of the simulation as its composition or total mass change; the particles are not "tagged" with a constant weight.

Again, we stress that the purpose of this weighting scheme is to reduce ensemble variance, and we computationally over-represent the rare but important particles and under-represent the common and less important particles. As we show below, this tradeoff significantly improves performance.

The idea of weighting particles has been put forward in various diverse forms by, e.g., Babovsky [20], Eibeck and Wagner [21–25], Kolodko and Sabelfeld [26], Shima et al. [19], Irizarry [27,28], Wells and Kraft [29], Zhao et al. [30], Zhao and Zheng [31], Zhao et al. [32], and Debry et al. [33]. Our approach is most similar in spirit to that of Kolodko and Sabelfeld [26]; what was considered there was a class of algorithms for pure coagulational processes, and what we do here is present a broad generalization of their family of algorithms for coagulation coupled to the other processes we consider. A large number of papers have considered the Mass Flow Algorithm (MFA) applied to a wide variety of physical problems [21–25,29,34–38]; we show below that the MFA algorithm is one of the members of the family that we consider below. Another approach is the multi-Monte Carlo method [30–32,39] which introduces a splitting scheme very similar to ours but has proposed a different class of weighting schemes.

After we introduce and analyze this family of weighting and splitting schemes, we quantify the performance of using different weighting functions by applying the Weighted Flow Algorithm to the recently-developed particle-resolved model PartMC-MOSAIC [14,2]. PartMC is a Lagrangian box model that explicitly stores the composition of many individual aerosol particles within a well-mixed computational volume. Relative particle positions within this computational volume are not tracked, but rather the coagulation process is simulated stochastically by assuming that coagulation events are Poisson distributed with a Brownian kernel. Apart from coagulation, the processes of particle emissions from various sources and dilution with the background are treated stochastically. PartMC was coupled with the aerosol chemistry model MOSAIC [2], which simulates the gas and particle phase chemistries, particle phase thermodynamics, and dynamic gas-particle mass transfer in a deterministic manner. The coupled model system, PartMC-MOSAIC, predicts number, mass, and full composition distributions of the aerosol populations. The current version of PartMC is available under the GNU General Public License (GPL) at http://lagrange.mechse.illinois.edu/mwest/partmc/, and the MOSAIC code is available upon request from Zaveri.

We use the urban plume scenario described in Zaveri et al. [11] where we simulated the evolution of the mixing state of an aerosol population in a polluted environment. We show that choosing weighting functions of the form $W(\mu) = \mu^\alpha$ can greatly increase the accuracy and performance of the total simulation, and that different values of α are optimal for different observables.

This manuscript is organized as follows. In Section 2 we present the governing equations for the coupled gas-aerosol box model and discuss the approximations needed by this model of the physical system. Section 3 introduces the weighted particle methods. Section 4 describes the mathematical formalism of weighted particle methods for coagulation and condensation. In Section 5 we present the weighted flow algorithms (WFA) as implemented in PartMC. Finally, Section 6 presents the application of PartMC-MOSAIC using WFA to the urban plume scenario. A list of symbols used in the paper is provided in Table A.2.

2. Continuous model system equations

We model a Lagrangian air parcel containing gas species and aerosol particles. We assume that environmental parameters and gas concentrations are homogeneous within the parcel and we do not track aerosol particle locations.

Each aerosol particle is described by a vector $\boldsymbol{\mu} \in \mathbb{R}^A$ with the ath component $\mu^a \geqslant 0$ giving the mass of species a. For a population of aerosol particles we denote by $N(\boldsymbol{\mu}, t)$ the cumulative aerosol number distribution at time t and constituent masses $\boldsymbol{\mu} \in \mathbb{R}^A$, which is defined to be the number concentration of aerosol particles that contain less than μ^a mass of species a, for all $a = 1, \ldots, A$. The aerosol number distribution $n(\boldsymbol{\mu}, t)$ at time t and constituent masses $\boldsymbol{\mu} \in \mathbb{R}^A$ is then is defined by

$$n(\boldsymbol{\mu}, t) = \frac{\partial^A N(\boldsymbol{\mu}, t)}{\partial \mu^1 \partial \mu^2 \ldots \partial \mu^A}. \tag{1}$$

Aerosol particles undergo Brownian coagulation, modeled by the coagulation kernel $K(\boldsymbol{\mu}, \boldsymbol{\nu})$ between particles with constituent masses $\boldsymbol{\mu}$ and $\boldsymbol{\nu}$. Emissions of aerosol particles into the air parcel are described by the number distribution rate $\dot{n}_{\text{emit}}(\boldsymbol{\mu}, t)$ and dilution with a background aerosol number distribution $n_{\text{back}}(\boldsymbol{\mu}, t)$ occurs at rate $\lambda_{\text{dil}}(t)$.

The gas species in the air parcel are described by the vector $\boldsymbol{g}(t) \in \mathbb{R}^G$ of gas species concentrations. The gas concentration growth rate due to gas chemical reactions is given by $\boldsymbol{R}(\boldsymbol{g})$, the gas emission rate is $\dot{\boldsymbol{g}}_{\text{emit}}(t)$, and the background gas concentrations are $\boldsymbol{g}_{\text{back}}(t)$.

The first C aerosol and gas species undergo gas-particle exchange, so gas species a converts to and from aerosol species a, for $a = 1, \ldots, C$. This exchange is described by the gas-to-particle flux-rate vector $\boldsymbol{I}(\boldsymbol{\mu}, \boldsymbol{g}, t) \in \mathbb{R}^G$ (with $I^a(\boldsymbol{\mu}, \boldsymbol{g}, t) = 0$ for $a > C$) and the water-particle flux rate $I^{\text{w}}(\boldsymbol{\mu}, \boldsymbol{g}, t)$, together with the conversion factors c^a from gas concentrations to aerosol species mass concentrations and the conversion factor c^{w} for water. We assume aerosol water is aerosol species number $C + 1$.

The environmental parameters in the air parcel are temperature $T(t)$, pressure $p(t)$, relative humidity $\text{RH}(t)$, and dry air density $\rho_{\text{dry}}(t)$. We prescribe the air temperature as a function of time and keep the air pressure and water mixing ratio constant, updating the relative humidity and dry air density appropriately.

The model system is

$$\frac{\partial n(\boldsymbol{\mu}, t)}{\partial t} = \underbrace{\frac{1}{2} \int_{[\boldsymbol{0}, \boldsymbol{\mu}]} K(\boldsymbol{\nu}, \boldsymbol{\mu} - \boldsymbol{\nu}) n(\boldsymbol{\nu}, t) n(\boldsymbol{\mu} - \boldsymbol{\nu}, t) d\boldsymbol{\nu}}_{\text{coagulation gain}} - \underbrace{\int_{[\boldsymbol{0}, \infty]} K(\boldsymbol{\mu}, \boldsymbol{\nu}) n(\boldsymbol{\mu}, t) n(\boldsymbol{\nu}, t) d\boldsymbol{\nu}}_{\text{coagulation loss}} \tag{2a}$$

$$+ \underbrace{\dot{n}_{\text{emit}}(\boldsymbol{\mu}, t)}_{\text{emissions}} + \underbrace{\lambda_{\text{dil}}(t)(n_{\text{back}}(\boldsymbol{\mu}, t) - n(\boldsymbol{\mu}, t))}_{\text{dilution}} + \underbrace{\frac{1}{\rho_{\text{dry}}(t)} \frac{d\rho_{\text{dry}}(t)}{dt} n(\boldsymbol{\mu}, t)}_{\text{volume change}} \tag{2b}$$

$$- \underbrace{\sum_{a=1}^{C} \frac{\partial}{\partial \mu^a} (c^a I^a(\boldsymbol{\mu}, \boldsymbol{g}, t) n(\boldsymbol{\mu}, t))}_{\text{gas-particle exchange}} - \underbrace{\frac{\partial}{\partial \mu^{C+1}} (c^{\text{w}} I^{\text{w}}(\boldsymbol{\mu}, \boldsymbol{g}, t) n(\boldsymbol{\mu}, t))}_{\text{water-particle exchange}} \tag{2c}$$

$$\frac{d\boldsymbol{g}(t)}{dt} = \underbrace{\dot{\boldsymbol{g}}_{\text{emit}}(t)}_{\text{emissions}} + \underbrace{\lambda_{\text{dil}}(t)(\boldsymbol{g}_{\text{back}}(t) - \boldsymbol{g}(t))}_{\text{dilution}} + \underbrace{\frac{1}{\rho_{\text{dry}}(t)} \frac{d\rho_{\text{dry}}(t)}{dt} \boldsymbol{g}(t)}_{\text{volume change}} \tag{2d}$$

$$- \underbrace{\int_{[\boldsymbol{0}, \infty]} \boldsymbol{I}(\boldsymbol{\mu}, \boldsymbol{g}, t) n(\boldsymbol{\mu}, t) d\boldsymbol{\mu}}_{\text{gas-particle exchange}} + \underbrace{\boldsymbol{R}(\boldsymbol{g})}_{\text{chemical reactions}}, \tag{2e}$$

where $[\boldsymbol{0}, \boldsymbol{\mu}] = \{\boldsymbol{\nu} \in \mathbb{R}^A \mid 0 \leqslant \nu^a \leqslant \mu^a \text{ for } a = 1, \ldots, A\}$ is a rectangle in $\mathbb{R}^A$. The Eq. (2) must be augmented with appropriate boundary conditions, which are chosen on physical grounds to ensure that the constituent masses of particles cannot become negative and that mass is conserved. Many of the rates, coefficients and functions in (2) depend on the environmental conditions but we have not written this dependence explicitly.

3. Weighted particle methods and superparticles

To discretize the aerosol number distribution $n(\boldsymbol{\mu})$ at a given instant of time within the Lagrangian air parcel, we can sample a finite number N_{p} of computational particles (written as a list $\Pi = \{\boldsymbol{\mu}_1, \boldsymbol{\mu}_2, \ldots, \boldsymbol{\mu}_{N_{\text{p}}}\}$) within a *computational volume* V. Multiple particles may have the same mass vector, making Π a multiset in the sense of Knuth [40, p. 473].

As we will see in Section 6, if each computational particle corresponds to the same number concentration, then this representation can give poor resolution for some measures of an aerosol distribution. For example, the mass distribution will tend to be under-sampled at larger masses, as only a few large particles will be present in the sample.

To mitigate this problem we weight each computational particle by a *weighting function* $W(\boldsymbol{\mu})$, so that the computational particle collection Π gives an approximate number distribution by

$$n(\boldsymbol{\mu}) = \frac{1}{V}\sum_{i=1}^{N_p} W(\boldsymbol{\mu}_i)\delta(\boldsymbol{\mu}-\boldsymbol{\mu}_i), \tag{3}$$

where $\delta(\boldsymbol{\mu})$ is the Dirac delta function. Particular cases of such weightings have been used previously, for example in the Mass Flow Algorithm [20–25] which weights particles in inverse proportion to their total mass.

In this paper we derive general algorithms for coagulation and gas-particle exchange with arbitrary weighting functions. For our numerical investigations in Section 6, however, we focus on weighting functions of the form

$$W(\boldsymbol{\mu}) = \left(\frac{D(\boldsymbol{\mu})}{D_0}\right)^{\alpha}, \tag{4}$$

where $D(\boldsymbol{\mu})$ is the diameter of the particle $\boldsymbol{\mu}$, $\alpha \in \mathbb{R}$ is a constant exponent, and D_0 is a reference diameter. The choice of α controls whether larger particles are weighted more or less than smaller particles, and the extent to which this occurs. For a given α, the product $(D_0)^{\alpha}V$ determines the overall scaling of (3) and in practice we determine this by the choice of the initial number of computational particles.

While we track every particle within the computational volume V, we regard this volume as being representative of a much larger air parcel. For example, in Section 6 we use a computational volume on the order of a few cubic centimeters but take this to be approximating the state of the well-mixed boundary layer during the day and the residual layer during the night.

The simulation of the aerosol state proceeds by two mechanisms. First, the composition of each particle can change, changing the components of the vector $\boldsymbol{\mu}$ as species condense from the gas phase and evaporate to it, for example. Second, the population Π can have particles added and removed, either by emissions, dilution, or coagulation events between particles.

4. Particle evolution equations

In this section we will describe the mathematical formalism behind a particle method algorithm which takes coagulation and advection into account in a systematic way. We will motivate each of these two ideas separately: in Section 4.1 we describe how to develop a weighted particle method for pure coagulation processes and in Section 4.2 we consider pure advection processes.

4.1. Particle equations for coagulation

We want to derive a particle method which will correctly simulate the continuous Smoluchowski equation with a weighting. We break this exposition into three steps: we will first compute the effect of changing variables on the continuous Smoluchowski equation, we will then rewrite this new equation in such a way as to heuristically justify the splitting method we will employ, and finally we will define a splitting method for particle Markov Chain models inspired by this heuristic and determine the optimal algorithm in this class. This will be the algorithm which we use to compute the results in Section 6.

Step 1. Continuous change of variables of continuous Smoluchowski equation. For the mass $\boldsymbol{\mu}$ and number concentration $n(\boldsymbol{\mu})$, the Smoluchowski coagulation equation is

$$\frac{\partial n(\boldsymbol{\mu})}{\partial t} = \frac{1}{2}\int_{[\mathbf{0},\boldsymbol{\mu}]} K(\boldsymbol{\nu},\boldsymbol{\mu}-\boldsymbol{\nu})n(\boldsymbol{\nu})n(\boldsymbol{\mu}-\boldsymbol{\nu})d\boldsymbol{\nu} - \int_{[\mathbf{0},\infty]} K(\boldsymbol{\nu},\boldsymbol{\mu})n(\boldsymbol{\nu})n(\boldsymbol{\mu})d\boldsymbol{\nu}, \tag{5}$$

where $K(\boldsymbol{\mu},\boldsymbol{\nu})$ is the coagulation rate between particles of masses $\boldsymbol{\mu}$ and $\boldsymbol{\nu}$. Let $W(\boldsymbol{\mu})$ be a weighting function and take $n(\boldsymbol{\mu}) = W(\boldsymbol{\mu})c(\boldsymbol{\mu})$, where $c(\boldsymbol{\mu})$ is the "computational number" concentration. Then

$$W(\boldsymbol{\mu})\frac{\partial c(\boldsymbol{\mu})}{\partial t} = \frac{1}{2}\int_{[\mathbf{0},\boldsymbol{\mu}]} K(\boldsymbol{\nu},\boldsymbol{\mu}-\boldsymbol{\nu})W(\boldsymbol{\nu})c(\boldsymbol{\nu})W(\boldsymbol{\mu}-\boldsymbol{\nu})c(\boldsymbol{\mu}-\boldsymbol{\nu})d\boldsymbol{\nu} - \int_{[\mathbf{0},\infty]} K(\boldsymbol{\nu},\boldsymbol{\mu})W(\boldsymbol{\nu})c(\boldsymbol{\nu})W(\boldsymbol{\mu})c(\boldsymbol{\mu})d\boldsymbol{\nu}, \tag{6}$$

$$\frac{\partial c(\boldsymbol{\mu})}{\partial t} = \frac{1}{2}\int_{[\mathbf{0},\boldsymbol{\mu}]} \frac{K(\boldsymbol{\nu},\boldsymbol{\mu}-\boldsymbol{\nu})W(\boldsymbol{\nu})W(\boldsymbol{\mu}-\boldsymbol{\nu})}{W(\boldsymbol{\mu})}c(\boldsymbol{\nu})c(\boldsymbol{\mu}-\boldsymbol{\nu})d\boldsymbol{\nu} - \int_{[\mathbf{0},\infty]} K(\boldsymbol{\nu},\boldsymbol{\mu})W(\boldsymbol{\nu})c(\boldsymbol{\nu})c(\boldsymbol{\mu})d\boldsymbol{\nu}. \tag{7}$$

Step 2. Heuristic motivation for splitting method. Assume that $W(\boldsymbol{\mu})$ is a non-increasing function. Define $L(\boldsymbol{\mu},\boldsymbol{\nu})$ by

$$L(\boldsymbol{\mu},\boldsymbol{\nu}) = K(\boldsymbol{\mu},\boldsymbol{\nu})\frac{W(\boldsymbol{\mu})W(\boldsymbol{\nu})}{W(\boldsymbol{\mu}+\boldsymbol{\nu})}, \tag{8}$$

or

$$K(\boldsymbol{\mu},\boldsymbol{\nu})W(\boldsymbol{\mu}) = L(\boldsymbol{\mu},\boldsymbol{\nu})\frac{W(\boldsymbol{\mu}+\boldsymbol{\nu})}{W(\boldsymbol{\nu})}. \tag{9}$$

Then (7) becomes

$$\frac{\partial c(\boldsymbol{\mu})}{\partial t} = \frac{1}{2}\int_{[\mathbf{0},\boldsymbol{\mu}]} L(\boldsymbol{\nu},\boldsymbol{\mu}-\boldsymbol{\nu})c(\boldsymbol{\nu})c(\boldsymbol{\mu}-\boldsymbol{\nu})d\boldsymbol{\nu} - \int_{[\mathbf{0},\infty]} L(\boldsymbol{\nu},\boldsymbol{\mu})\frac{W(\boldsymbol{\mu}+\boldsymbol{\nu})}{W(\boldsymbol{\mu})}c(\boldsymbol{\nu})c(\boldsymbol{\mu})d\boldsymbol{\nu}. \tag{10}$$

This equation is of a similar type to that of a Smoluchowski equation, but the creation kernel differs from the destruction kernel. Interpreting (10) as the mean of a particle process leads to a probabilistic interpretation: particles of size $\boldsymbol{\mu}$ are created from collisions between particles of size $\boldsymbol{\mu}-\boldsymbol{\nu}$ and $\boldsymbol{\nu}$ with rate $L(\boldsymbol{\nu},\boldsymbol{\mu}-\boldsymbol{\nu})$, and are destroyed by collisions with particles of size $\boldsymbol{\nu}$ with rate $L(\boldsymbol{\nu},\boldsymbol{\mu})W(\boldsymbol{\mu}+\boldsymbol{\nu})/W(\boldsymbol{\mu})$. Writing it as in (10) is another way of thinking of the creation and destruction processes as the culmination of a *two-step* process: the first step corresponds to *choosing a triplet of particles* $(m,n,m+n)$ on which an event may or may not occur; the second step corresponds to deciding if an event (or events) did or did not occur involving this triplet. For example, to destroy a particle of size $\boldsymbol{\mu}$ through a collision with a particle of size $\boldsymbol{\nu}$, we first need to choose a triplet involving $\boldsymbol{\mu}$ as one of the two smaller particles, and we choose the triplet $(\boldsymbol{\mu},\boldsymbol{\nu},\boldsymbol{\mu}+\boldsymbol{\nu})$ with rate $L(\boldsymbol{\nu},\boldsymbol{\mu})$, and we then destroy particle $\boldsymbol{\mu}$ with probability $p_{\text{death}} = W(\boldsymbol{\mu}+\boldsymbol{\nu})/W(\boldsymbol{\mu})$. This is a **split method** where we choose the first event in the standard way for a continuous-time Markov process, and the second as for a discrete-time Markov process, but used the combined process as a proxy for one continuous-time process whose rate is given by the product (see, e.g. Proposition 4.5 of [41]). We have used here that the weighting function W is non-increasing, so that the ratio of W's in the destruction integral in (10) is always less than one. We deal with the case of a more general form of W now.

Step 3. Splitting method Assume that we have a class of Markov particle processes involving interactions such that the kernel is "coagulation-like" and symmetric, i.e. every reaction involves the triplet $\boldsymbol{\mu}$, $\boldsymbol{\nu}$, $\boldsymbol{\mu}+\boldsymbol{\nu}$, and the rate of every such reaction must be unchanged under a switch of $\boldsymbol{\mu}$ and $\boldsymbol{\nu}$.

We can describe all creation or destruction events by two successive steps: the first step corresponds to choosing a triple of particles which may undergo a reaction, and the second is deciding whether the events actually occur. We assume a rate $R(\boldsymbol{\mu},\boldsymbol{\nu})$ which corresponds to the triplet $(\boldsymbol{\mu},\boldsymbol{\nu},\boldsymbol{\mu}+\boldsymbol{\nu})$ *potentially* having a reaction; once this triplet has been chosen, we choose three independent events after this: we create the product particle $\boldsymbol{\mu}+\boldsymbol{\nu}$ with probability $p_{\text{birth}}(\boldsymbol{\mu},\boldsymbol{\nu})$, we destroy particle $\boldsymbol{\mu}$ with probability $p_{\text{death}}(\boldsymbol{\nu},\boldsymbol{\mu})$, and we destroy particle $\boldsymbol{\nu}$ with probability $p_{\text{death}}(\boldsymbol{\mu},\boldsymbol{\nu})$. In this formulation, once a triplet has been chosen, any of eight possibilities can occur. (We have made the assumption here that each of the three individual events are chosen independently but cf. the appendix where we consider an even more general method.)

It has been shown by Norris 42, Theorem 4.1 that the direct particle method for the standard unweighted Smoluchowski equation converges in a certain precise sense to its formal $N_p \to \infty$ limit (5). We will simply use the formal large N_p limit in this paper, but will prove that this converges in the same sense in later work [43]. This formal large-N_p limit for c is:

$$\frac{\partial c(\boldsymbol{\mu})}{\partial t} = \frac{1}{2}\int_{[\mathbf{0},\boldsymbol{\mu}]} R(\boldsymbol{\nu},\boldsymbol{\mu}-\boldsymbol{\nu})p_{\text{birth}}(\boldsymbol{\nu},\boldsymbol{\mu}-\boldsymbol{\nu})c(\boldsymbol{\nu})c(\boldsymbol{\mu}-\boldsymbol{\nu})d\boldsymbol{\nu} - \int_0^\infty R(\boldsymbol{\nu},\boldsymbol{\mu})p_{\text{death}}(\boldsymbol{\nu},\boldsymbol{\mu})c(\boldsymbol{\nu})c(\boldsymbol{\mu})d\boldsymbol{\nu}. \tag{11}$$

We have some freedom still in choosing R, p_{birth}, p_{death}; we will require them to satisfy the following two algorithmic conditions:

1. Consistency: match large-N limit equations: equate Eqs. (7) and (11).
2. Optimality: maximize p_{death} and p_{birth}.

The motivation for this optimality condition is clear: the smaller p_{birth} and p_{death} are, the more "wasted" steps we will have, i.e. cases where we choose triplets and then do not actually have a creation or destruction event. Maximizing these quantities will then lead to the smallest number of wasted events. As we see below, it is possible to maximize both simultaneously.

Theorem 4.1. *There is a unique optimal variable-resolution particle method, i.e. a unique choice of R, p_{birth}, p_{death} which satisfy the two algorithmic conditions, namely by choosing:*

$$R(\boldsymbol{\mu},\boldsymbol{\nu}) = K(\boldsymbol{\mu},\boldsymbol{\nu})\frac{W(\boldsymbol{\mu})W(\boldsymbol{\nu})}{W_{\min}(\boldsymbol{\mu},\boldsymbol{\nu})}, \tag{12a}$$

$$p_{\text{death}}(\boldsymbol{\mu},\boldsymbol{\nu}) = \frac{W_{\min}(\boldsymbol{\mu},\boldsymbol{\nu})}{W(\boldsymbol{\nu})}, \tag{12b}$$

$$p_{\text{birth}}(\boldsymbol{\mu},\boldsymbol{\nu}) = \frac{W_{\min}(\boldsymbol{\mu},\boldsymbol{\nu})}{W(\boldsymbol{\mu}+\boldsymbol{\nu})}, \tag{12c}$$

$$W_{\min}(\boldsymbol{\mu},\boldsymbol{\nu}) = \min(W(\boldsymbol{\mu}),W(\boldsymbol{\nu}),W(\boldsymbol{\mu}+\boldsymbol{\nu})). \tag{12d}$$

Proof. Comparing Eqs. (7) and (11) gives

$$R(\boldsymbol{\nu}, \boldsymbol{\mu}-\boldsymbol{\nu}) p_{\text{birth}}(\boldsymbol{\nu}, \boldsymbol{\mu}-\boldsymbol{\nu}) = \frac{K(\boldsymbol{\nu}, \boldsymbol{\mu}-\boldsymbol{\nu}) W(\boldsymbol{\nu}) W(\boldsymbol{\mu}-\boldsymbol{\nu})}{W(\boldsymbol{\mu})},$$
$$R(\boldsymbol{\nu}, \boldsymbol{\mu}) p_{\text{death}}(\boldsymbol{\nu}, \boldsymbol{\mu}) = K(\boldsymbol{\nu}, \boldsymbol{\mu}) W(\boldsymbol{\nu}).$$

Rearranging these gives:

$$p_{\text{birth}}(\boldsymbol{\nu}, \boldsymbol{\mu}) = \frac{K(\boldsymbol{\nu}, \boldsymbol{\mu}) W(\boldsymbol{\nu}) W(\boldsymbol{\mu})}{R(\boldsymbol{\nu}, \boldsymbol{\mu}) W(\boldsymbol{\nu}+\boldsymbol{\mu})},$$
$$p_{\text{death}}(\boldsymbol{\nu}, \boldsymbol{\mu}) = \frac{K(\boldsymbol{\nu}, \boldsymbol{\mu}) W(\boldsymbol{\nu})}{R(\boldsymbol{\nu}, \boldsymbol{\mu})}.$$

As both p_{birth} and p_{death} are inversely proportional to R, maximizing the probabilities corresponds to minimizing R. We thus wish to minimize $R(\nu, \mu)$ subject to

$$p_{\text{birth}}(\boldsymbol{\mu}, \boldsymbol{\nu}) = p_{\text{birth}}(\boldsymbol{\nu}, \boldsymbol{\mu}) = \frac{K(\boldsymbol{\nu}, \boldsymbol{\mu}) W(\boldsymbol{\nu}) W(\boldsymbol{\mu})}{R(\boldsymbol{\nu}, \boldsymbol{\mu}) W(\boldsymbol{\nu}+\boldsymbol{\mu})} \leqslant 1,$$
$$p_{\text{death}}(\boldsymbol{\nu}, \boldsymbol{\mu}) = \frac{K(\boldsymbol{\nu}, \boldsymbol{\mu}) W(\boldsymbol{\nu})}{R(\boldsymbol{\nu}, \boldsymbol{\mu})} \leqslant 1,$$
$$p_{\text{death}}(\boldsymbol{\mu}, \boldsymbol{\nu}) = \frac{K(\boldsymbol{\mu}, \boldsymbol{\nu}) W(\boldsymbol{\mu})}{R(\boldsymbol{\mu}, \boldsymbol{\nu})} \leqslant 1.$$

Symmetry of K and R means that this is equivalent to

$$\max\left(\frac{K(\boldsymbol{\nu}, \boldsymbol{\mu}) W(\boldsymbol{\nu}) W(\boldsymbol{\mu})}{R(\boldsymbol{\nu}, \boldsymbol{\mu}) W(\boldsymbol{\nu}+\boldsymbol{\mu})}, \frac{K(\boldsymbol{\nu}, \boldsymbol{\mu}) W(\boldsymbol{\nu})}{R(\boldsymbol{\nu}, \boldsymbol{\mu})}, \frac{K(\boldsymbol{\nu}, \boldsymbol{\mu}) W(\boldsymbol{\mu})}{R(\boldsymbol{\nu}, \boldsymbol{\mu})}\right) \leqslant 1,$$

which in turn is equivalent to

$$R(\boldsymbol{\nu}, \boldsymbol{\mu}) \geqslant K(\boldsymbol{\nu}, \boldsymbol{\mu}) \max\left(\frac{W(\boldsymbol{\nu}) W(\boldsymbol{\mu})}{W(\boldsymbol{\nu}+\boldsymbol{\mu})}, W(\boldsymbol{\nu}), W(\boldsymbol{\mu})\right) = K(\boldsymbol{\nu}, \boldsymbol{\mu}) W(\boldsymbol{\nu}) W(\boldsymbol{\mu}) \max\left(\frac{1}{W(\boldsymbol{\nu}+\boldsymbol{\mu})}, \frac{1}{W(\boldsymbol{\mu})}, \frac{1}{W(\boldsymbol{\nu})}\right)$$
$$= \frac{K(\boldsymbol{\nu}, \boldsymbol{\mu}) W(\boldsymbol{\nu}) W(\boldsymbol{\mu})}{W_{\min}(\boldsymbol{\nu}, \boldsymbol{\mu})}. \tag{13}$$

To minimize $R(\nu, \mu)$ we thus take it equal to (13), giving the expressions (12). □

4.1.1. Connections to the Mass Flow Algorithm

The weighted scheme we propose above is reminiscent of the Mass-Flow Algorithm (MFA) used by Babovsky [20] and Eibeck and Wagner [21–25] and is a non-symmetric particle method similar to our scheme with $W(D) \propto D^{-3}$. The algorithm is as follows: first the triplet $(\boldsymbol{\mu}, \boldsymbol{\nu}, \boldsymbol{\mu}+\boldsymbol{\nu})$ is chosen with rate

$$Q(\boldsymbol{\mu}, \boldsymbol{\nu}) = K(\boldsymbol{\mu}, \boldsymbol{\nu})\left(\frac{1}{\mu} + \frac{1}{\nu}\right), \tag{14}$$

where here and below we denote $\mu = |\boldsymbol{\mu}| = \sum_{a=1}^{A} \mu^a$ as the total mass of a particle with species mass vector $\boldsymbol{\mu}$. (Babovsky [20] and Eibeck and Wagner [21–25] only considered *scalar* coagulation equations, i.e. assumed that the independent variable in the coagulation equation was one-dimensional, but the extension to the vector-valued case is straightforward.)

After the triplet is chosen, the algorithm *always* adds the particle $\boldsymbol{\mu}+\boldsymbol{\nu}$ to the population, and then kills exactly one of the $\boldsymbol{\mu}$ or $\boldsymbol{\nu}$. With probability $\mu/(\mu+\nu)$ the particle $\boldsymbol{\mu}$ is removed, otherwise the particle $\boldsymbol{\nu}$ is removed. Note that this algorithm *always adds the coagulated particle* and always kills *exactly one* of the initial particles.

If we compare the MFA with our algorithm choosing a weighting of $W(\boldsymbol{\mu}) = 1/\mu$, we have $W_{\min}(\boldsymbol{\mu}, \boldsymbol{\nu}) = W(\boldsymbol{\mu}+\boldsymbol{\nu}) = 1/(\mu+\nu)$ and so Eq. (12) become

$$R(\boldsymbol{\mu}, \boldsymbol{\nu}) = K(\boldsymbol{\mu}, \boldsymbol{\nu}) \frac{(1/\mu)(1/\nu)}{1/(\mu+\nu)} = K(\boldsymbol{\mu}, \boldsymbol{\nu}) \frac{\mu+\nu}{\mu\nu} = Q(\boldsymbol{\mu}, \boldsymbol{\nu}), \tag{15a}$$
$$p_{\text{death}}(\boldsymbol{\mu}, \boldsymbol{\nu}) = \frac{\nu}{\mu+\nu}, \tag{15b}$$
$$p_{\text{death}}(\boldsymbol{\nu}, \boldsymbol{\mu}) = \frac{\mu}{\mu+\nu}, \tag{15c}$$
$$p_{\text{birth}}(\boldsymbol{\mu}, \boldsymbol{\nu}) = 1. \tag{15d}$$

Note that these are the same average rates as the MFA and will give the same mean (large N) behavior. The difference is that the two constituent particles are removed with independent probabilities, rather than always one or the other being removed as in the MFA. In Appendix A.2 we show how generalizing our method to non-symmetric interactions exactly recovers MFA as a special case.

4.2. Advection for gas-particle exchange

Let $\boldsymbol{v}(\boldsymbol{\mu},t)$ be the mass change rate of particles of mass vector $\boldsymbol{\mu}$ at time t, so that the mass of a particle, $\boldsymbol{\mu}(t)$, satisfies the differential equation

$$\frac{d}{dt}\boldsymbol{\mu}(t) = \boldsymbol{v}(\boldsymbol{\mu}(t),t). \tag{16}$$

Define $\Phi(\boldsymbol{\mu},t_0,t)$ to be the flow map for the vector field $\boldsymbol{v}(\boldsymbol{\mu},t)$, i.e. for $t > t_0$,

$$\frac{\partial}{\partial t}\Phi(\boldsymbol{\mu},t_0,t) = \boldsymbol{v}(\Phi(\boldsymbol{\mu},t_0,t),t), \tag{17a}$$

$$\Phi(\boldsymbol{\mu},t_0,t_0) = \boldsymbol{\mu}. \tag{17b}$$

As the masses of particles change according to the rate $\boldsymbol{v}(\boldsymbol{\mu},t)$, the number distribution $n(\boldsymbol{\mu},t)$ evolves by

$$\frac{d}{dt}n(\boldsymbol{\mu},t) + \nabla_{\boldsymbol{\mu}}(\boldsymbol{v}(\boldsymbol{\mu},t)n(\boldsymbol{\mu},t)) = 0, \tag{18}$$

which can be solved by the method of characteristics to find the solution

$$n(\Phi(\boldsymbol{\mu},t_0,t),t) = n(\boldsymbol{\mu},t_0). \tag{19}$$

Now consider $n(\boldsymbol{\mu},t) = W(\boldsymbol{\mu})c(\boldsymbol{\mu},t)$, which implies

$$W(\Phi(\boldsymbol{\mu},t_0,t))c(\Phi(\boldsymbol{\mu},t_0,t),t) = W(\boldsymbol{\mu})c(\boldsymbol{\mu},t_0). \tag{20}$$

Let the "particle-attached number concentration" $q(\boldsymbol{\mu},t)$ be defined by

$$q(\boldsymbol{\mu},t) = c(\Phi(\boldsymbol{\mu},t_0,t),t), \tag{21}$$

which thus satisfies

$$W(\Phi(\boldsymbol{\mu},t_0,t))q(\boldsymbol{\mu},t) = W(\boldsymbol{\mu})q(\boldsymbol{\mu},t_0), \tag{22}$$

so

$$q(\boldsymbol{\mu},t) = \frac{W(\boldsymbol{\mu})}{W(\Phi(\boldsymbol{\mu},t_0,t))}q(\boldsymbol{\mu},t_0). \tag{23}$$

Note that $q(\boldsymbol{\mu},t)$ in (23) is not an integer. A consistent way to make this number integer is described in the next section.

4.2.1. Approximate particle method for advection

Given a list of particles $\Pi_t = \{\boldsymbol{\mu}_i(t)\}_{i=1}^{N_p(t)}$ that approximate $c(\boldsymbol{\mu},t)$ by

$$c(\boldsymbol{\mu},t) \approx \frac{1}{V}\sum_{i=1}^{N_p(t)}\delta(\boldsymbol{\mu}-\boldsymbol{\mu}_i(t)), \tag{24}$$

we evolve the solution of (23) by

$$\Pi_{t+\Delta t} = \biguplus_{k=1}^{N_p(t)} \Omega(\boldsymbol{\mu}_k,t,t+\Delta t)\otimes\{\Phi(\boldsymbol{\mu}_k(t),t,t+\Delta t)\}, \tag{25}$$

where we use the multiset notation [40, p. 473] with $n\otimes A$ denoting n concatenated copies of the list A and $A\uplus B$ denoting the concatenation of the lists A and B, and $\Omega(\boldsymbol{\mu},t,t+\Delta t)$ is an integer-valued random variable with expected value

$$r(\boldsymbol{\mu},t,t+\Delta t) = \frac{W(\boldsymbol{\mu})}{W(\Phi(\boldsymbol{\mu},t,t+\Delta t))}. \tag{26}$$

In practice, we take $\Omega(\boldsymbol{\mu},t)$ to be

$$\Omega(\boldsymbol{\mu},t,t+\Delta t) = \begin{cases} \lfloor r(\boldsymbol{\mu},t,t+\Delta t)\rfloor & \text{with probability } \lceil r(\boldsymbol{\mu},t,t+\Delta t)\rceil - r(\boldsymbol{\mu},t,t+\Delta t), \\ \lceil r(\boldsymbol{\mu},t,t+\Delta t)\rceil & \text{otherwise,} \end{cases} \tag{27}$$

where $\lfloor r\rfloor$ and $\lceil r\rceil$ are the floor and ceiling, respectively. This choice is computationally convenient since we can then write

$$\Omega(\boldsymbol{\mu},t,t+\Delta t) = \lfloor r(\boldsymbol{\mu},t,t+\Delta t) + U\rfloor \tag{28}$$

for U a uniformly $(0,1)$-distributed random variable. Moreover, we can see that in the limit $N_p\to\infty$, this approximation does not add any appreciable error: if we have $Q(\boldsymbol{\mu},t)$ particles of mass vector $\boldsymbol{\mu}$, then from (25), the number of particles of mass vector $\Phi(\boldsymbol{\mu},t,t+\Delta t)$ will be $\sum_{i=1}^{Q(\boldsymbol{\mu},t)}\Omega(\boldsymbol{\mu},t,t+\Delta t)$. This sum has mean $Q(\boldsymbol{\mu},t)r(\boldsymbol{\mu},t,t+\Delta t)$ and variance $Q(\boldsymbol{\mu},t)\sigma^2(\Omega(\boldsymbol{\mu},t,t+\Delta t))$. The choice of $\Omega(\mu,t,t+\Delta t)$ in (27) has variance

$$\sigma^2(\Omega(\boldsymbol{\mu},t,t+\Delta t)) = (\lceil r(\boldsymbol{\mu},t,t+\Delta t)\rceil - r(\boldsymbol{\mu},t,t+\Delta t))(r(\boldsymbol{\mu},t,t+\Delta t) - \lfloor r(\boldsymbol{\mu},t,t+\Delta t)\rfloor) < 1.$$

$Q(\boldsymbol{\mu},t)$ is itself a random quantity, but as long as the mean of $Q(\boldsymbol{\mu},t)$ is $c(\boldsymbol{\mu},t)$ and the variance of $Q(\boldsymbol{\mu},t) \sim N_p^{-1}$, then $\Omega(\boldsymbol{\mu},t,t+\Delta t) \otimes \Phi(\boldsymbol{\mu},t,t+\Delta t)$ has the correct mean $c(\boldsymbol{\mu},t)r(\boldsymbol{\mu},t,t+\Delta t)$ and variance which also scales like N_p^{-1}. By summation and independence this holds for the entire population.

4.3. Particle sampling for initial condition and emissions, and dilution

Because we use a finite number of particles to approximate the aerosol population, we need to add a finite number of emitted particles to the volume at each timestep. We assume that emissions are memoryless, so that emission of each particle is uncorrelated with emission of any other particle. Under this assumption the appropriate statistics are Poisson distributed, whereby the distribution of finite particles is parameterized by the mean emission rate and distribution.

Consider an emission rate $\dot{n}_{\text{emit}}(\boldsymbol{\mu},t)$ of particles as in the emission term of Eq. (2), a volume V, and a timestep Δt. The emissions over the timestep from time t_0 to $t_1 = t_0 + \Delta t$ are given by

$$n_{\text{emit}}(\boldsymbol{\mu};t_0,t_1) = \int_{t_0}^{t_1} \dot{n}_{\text{emit}}(\boldsymbol{\mu},t)dt \tag{29}$$

$$\approx \Delta t \dot{n}_{\text{emit}}(\boldsymbol{\mu},t_0) \tag{30}$$

for which we use the first-order approximation above.

For a weighting function $W(\boldsymbol{\mu})$, the corresponding computational number distribution and total computational number are

$$c_{\text{emit}}(\boldsymbol{\mu};t_0,t_1) = \frac{1}{W(\boldsymbol{\mu})} n_{\text{emit}}(\boldsymbol{\mu};t_0,t_1). \tag{31}$$

To obtain a finite Poisson sample of the number distribution $n_{\text{emit}}(\boldsymbol{\mu};t_0,t_1)$ in the computational volume V with the given weighting function, we first see that the total computational number concentration is

$$C_{\text{emit}}(t_0,t_1) = \int_{[\mathbf{0},\infty]} c_{\text{emit}}(\boldsymbol{\mu};t_0,t_1)d\boldsymbol{\mu}. \tag{32}$$

The actual number N_S of emitted computational particles added in a timestep will be Poisson distributed with mean $\lambda = C_{\text{emit}}(t_0,t_1)V$, written $N_S \sim \text{Pois}(\lambda)$.

A Poisson sampled population of emitted particles Π_{emit} of the emissions distribution $n_{\text{emit}}(\boldsymbol{\mu};t_0,t_1)$ in volume V, written $\Pi_{\text{samp}} \sim \text{Pois}_{\text{dist}}(n_{\text{emit}}(\cdot;t_0,t_1), V, W(\cdot))$, is a finite list of particles given by

$$\Pi_{\text{samp}} = \{\boldsymbol{\mu}_1, \boldsymbol{\mu}_2, \ldots, \boldsymbol{\mu}_{N_S}\}, \tag{33a}$$

$$N_S \sim \text{Pois}(C_{\text{emit}}(t_0,t_1)V), \tag{33b}$$

$$\boldsymbol{\mu}_i \sim \frac{c_{\text{emit}}(\boldsymbol{\mu};t_0,t_1)}{C_{\text{emit}}(t_0,t_1)} \quad \text{for } i = 1,\ldots,N_S, \tag{33c}$$

where (33c) means that each particle has a composition drawn from the normalization of the weighted number distribution $c_{\text{emit}}(\boldsymbol{\mu};t_0,t_1)$.

For simplicity we assume that for each source type the composition of the emitted particles is the same, e.g. for diesel exhaust particles we assume that they all consist of 70% black carbon and 30% primary organic carbon. We therefore only have to sample with respect to diameter D, for which we assume log-normal distributions:

$$n(D) = \frac{N}{\sqrt{2\pi}\log_{10}\sigma_g} \exp\left(-\frac{(\log_{10}D - \log_{10}D_{gn})^2}{2(\log_{10}\sigma_g)^2}\right), \tag{34}$$

where N is the number concentration, D_{gn} is the geometric mean diameter, and σ_g is the geometric standard deviation.

As mentioned before we consider weighting functions of the form

$$W(D) = \left(\frac{D}{D_0}\right)^{\alpha}, \tag{35}$$

where D_0 is a reference radius at which the weight will be 1, and α is the exponent. The weighted number concentration is thus

$$c(D) = \frac{n(D)}{W(D)}. \tag{36}$$

Rearranging this gives again a log-normal distribution

$$c(D) = \frac{N'}{\sqrt{2\pi}\log_{10}\sigma_g} \exp\left(-\frac{(\log_{10}D - \log_{10}D'_{gn})^2}{2(\log_{10}\sigma_g)^2}\right), \tag{37}$$

where the modified variables are

$$\log_{10}D'_{gn} = \log_{10}D_{gn} - \alpha(\log_{10}\sigma_g)^2 \ln(10), \tag{38}$$

$$N' = ND_0^{\alpha} \exp\left(-\alpha \ln(10)\log_{10}D_{gn} + \frac{\alpha^2}{2}(\ln(10))^2(\log_{10}\sigma_g)^2\right). \tag{39}$$

Similar arguments apply for the initial conditions and for the process of dilution.

5. Weighted Flow Algorithms (WFA)

The Weighted Flow Algorithms (WFA) for coagulation described in Section 4.1 can be implemented with any of the standard Gillespie-type methods [15–17,44] with the modified kernel (12a), requiring only the additional step of accepting death events for particle removal with probability (12b), and accepting birth events for new particles with probability (12c). For computational efficiency we implemented the WFA in an approximate fixed-timestep mode with a majorized explicit tau-leaping method Gillespie [45] performed on event groups induced by the particle population binned by particle diameter, as detailed in Algorithm 1.

This was incorporated into the PartMC-MOSAIC model system along with modifications for weighted particle population algorithms for emissions, dilution, gas-particle exchange, environmental changes, and gas chemistry, as outlined in Algorithm 2. These two algorithms can be contrasted with the unweighted versions described in Riemer et al. [14].

Algorithm 1: Weighted Flow Algorithm (WFA) for particle coagulation (constant-timestep size-binned version)

$\Pi = \{\boldsymbol{\mu}_i \in \mathbb{R}^A\}_{i=1}^{N_p}$ is the list of particle compositions
V is the computational volume
Δt is the timestep
$W(\boldsymbol{\mu})$ is the weighting function
$R(\boldsymbol{\mu}_1, \boldsymbol{\mu}_2)$ is the weighted kernel given by (12a) for the weighting function $W(\boldsymbol{\mu})$
divide the diameter axis into bins $[D_b, D_{b+1})$ as for a sectional model, for $b = 1, \ldots, N_{bin}$
$\Pi(b) = \{\boldsymbol{\mu} \in \Pi | D(\boldsymbol{\mu}) \in [D_b, D_{b+1})\}$ is the list of particles in bin b
$N_p(b) = |\Pi(b)|$ is the number of particles in bin b
$R_{max}(b_1, b_2)$ is an upper bound so $R(\boldsymbol{\mu}_1, \boldsymbol{\mu}_2) \leqslant R_{max}(b_1, b_2)$ for any particles $\boldsymbol{\mu}_1 \in \Pi(b_1)$ and $\boldsymbol{\mu}_2 \in \Pi(b_2)$
for all bin pairs (b_1, b_2) **do**
  $N_{event} \leftarrow N_p(b_1)(N_p(b_2) - \delta_{b_1,b_2})/2$
  randomly choose $N_{test} \sim \text{Pois}(R_{max}(b_1, b_2)\Delta t\, N_{event}/V)$
  for N_{test} repetitions **do**
    randomly choose distinct particles $\boldsymbol{\mu}_1 \in \Pi(b_1)$ and $\boldsymbol{\mu}_2 \in \Pi(b_2)$ independently and uniformly
    $W_{min} \leftarrow \min(W(\boldsymbol{\mu}_1), W(\boldsymbol{\mu}_2), W(\boldsymbol{\mu}_1 + \boldsymbol{\mu}_2))$
    randomly choose r, r_1, r_2, and r_3 independently and uniformly in $(0,1)$
    if $r < R(\boldsymbol{\mu}_1, \boldsymbol{\mu}_2)/R_{max}(b_1, b_2)$ **then**
      if $r_1 < W_{min}/W(\boldsymbol{\mu}_1)$ **then**
        remove particle $\boldsymbol{\mu}_1$, so that $\Pi \leftarrow \Pi \backslash \{\boldsymbol{\mu}_1\}$
      end if
      if $r_2 < W_{min}/W(\boldsymbol{\mu}_2)$ **then**
        remove particle $\boldsymbol{\mu}_2$, so that $\Pi \leftarrow \Pi \backslash \{\boldsymbol{\mu}_2\}$
      end if
      if $r_3 < W_{min}/W(\boldsymbol{\mu}_1 + \boldsymbol{\mu}_2)$ **then**
        add a new particle with mass vector $\boldsymbol{\mu}_{coag} = \boldsymbol{\mu}_1 + \boldsymbol{\mu}_2$, so that $\Pi \leftarrow \Pi \uplus \{\boldsymbol{\mu}_{coag}\}$
      end if
    end if
  end for
end for

Algorithm 2: Coupled PartMC-MOSAIC algorithm with variable weighting

$\Pi = \{\boldsymbol{\mu}_i \in \mathbb{R}^A\}_{i=1}^{N_p}$ is the list of particle compositions
V is the computational volume
Δt is the timestep
$W(\boldsymbol{\mu})$ is the weighting function
$\boldsymbol{g}$ is the gas concentrations
$t \leftarrow 0$
while $t < t_{\text{final}}$ **do**
  $t \leftarrow t + \Delta t$
  update temperature $T(t)$, pressure $p(t)$, relative humidity $\text{RH}(t)$, dry air density $\rho_{\text{dry}}(t)$, and mixing height $H(t)$
  $V(t) \leftarrow V(t - \Delta t)\frac{\rho_{\text{dry}}(t-\Delta t)}{\rho_{\text{dry}}(t)}$
  $\boldsymbol{g}(t) \leftarrow \boldsymbol{g}(t - \Delta t)\frac{\rho_{\text{dry}}(t)}{\rho_{\text{dry}}(t-\Delta t)}$
  perform one Δt-timestep of coagulation for Π with the WFA algorithm in Algorithm 1
  add $\Delta t\dot{\boldsymbol{g}}_{\text{emit}}(t) + \Delta t\lambda_{\text{dil}}(t)(\boldsymbol{g}_{\text{back}}(t) - \boldsymbol{g}(t))$ to $\boldsymbol{g}$
  randomly choose $N_{\text{loss}} \sim \text{Pois}(\Delta t\lambda_{\text{dil}}N_p)$ and remove N_{loss} randomly chosen particles from Π
  add a sample of $\text{Pois}_{\text{dist}}(\lambda_{\text{dil}}\Delta t\, n_{\text{back}}(\cdot, t), V, W(\cdot))$ to Π
  add a sample of $\text{Pois}_{\text{dist}}(\Delta t\dot{n}_{\text{emit}}(\cdot, t), V, W(\cdot))$ to Π
  integrate the system of coupled ODEs (2c) and (2e) with MOSAIC for time Δt, transforming each particle $\boldsymbol{\mu}_i$ to $\boldsymbol{\mu}_i'$
  for all particles $\boldsymbol{\mu}_i$ in Π **do**
    choose r uniformly in $(0,1)$
    $N_{\text{copies}} \leftarrow \lfloor W(\boldsymbol{\mu}_i')/W(\boldsymbol{\mu}_i) + r \rfloor$
    replace $\boldsymbol{\mu}_i$ in Π with N_{copies} of $\boldsymbol{\mu}_i'$, so that $\Pi \leftarrow (\Pi \setminus \{\boldsymbol{\mu}_i\}) \uplus (N_{\text{copies}} \otimes \boldsymbol{\mu}_i')$
  end for
    output data for time t
end while

6. Numerical results

6.1. Aerosol distribution functions

To facilitate the discussion of the results we define the following quantities: We take $N(D)$ to be the cumulative number distribution, giving the number of particles per volume that have diameter less than D. Similarly, the cumulative dry mass distribution $M(D)$ gives the dry mass per volume of particles with diameter less than D. We write $N = N(\infty)$ and $M = M(\infty)$, for the total number and dry mass concentrations, respectively. Given the cumulative distributions, we define the number distribution $n(D)$ and the mass distribution $m(D)$ as functions of diameter (wet or dry) by

$$n(D) = \frac{dN(D)}{d\log_{10}D}, \tag{40}$$

$$m(D) = \frac{dM(D)}{d\log_{10}D}. \tag{41}$$

To discuss the composition of a particle, we refer to the BC mass fractions, as

$$w_{\text{BC}} = \frac{\mu_{\text{BC}}}{\mu_{\text{dry}}}, \tag{42}$$

where μ_{BC} is the BC mass in a given particle, μ_{all} is the total wet mass of the particle, and $\mu_{\text{dry}} = \mu_{\text{all}} - \mu_{\text{H}_2\text{O}}$ is the total dry mass.

The number and mass concentrations can be further extended to be functions of both particle composition and diameter. That is, the two-dimensional cumulative number distribution $N(D, w_{\text{BC}})$ is the number of particles per volume that have a diameter less than D and a BC mass fraction less than w_{BC}. The two-dimensional number distribution $n(D, w_{\text{BC}})$ is then defined by

$$n(D, w_{\text{BC}}) = \frac{\partial^2 N(D, w_{\text{BC}})}{\partial\log_{10}D\partial w_{\text{BC}}}. \tag{43}$$

The two-dimensional cumulative total mass distribution $M(D, w_{\text{BC}})$ and mass distribution $m(D, w_{\text{BC}})$ are defined similarly. As well as the total mass we are also interested in the BC mass, so we define $M^{\text{BC}}(D, w_{\text{BC}})$ to be the total BC mass concentration from particles with diameter less than D and a BC mass fraction less than w_{BC}, with the corresponding BC mass distribution $m^{\text{BC}}(D, w_{\text{BC}})$.

To plot a two-dimensional distribution we formed a two-dimensional histogram by taking bins on both D and w_{BC} axes and counting the number or mass of particles that fall within each bin pair. These quantities were then plotted as a color-map, with no color if no particles were present in a given bin pair.

6.2. Statistics of the ensemble

Given R realizations $X_1, X_2, \ldots, X_R$ of a random variable X, we denote the sample mean by $\langle X \rangle$, the sample standard deviation by $\sigma(X)$, and the sample coefficient of variation by $\mathrm{CV}(X)$. Thus

$$\langle X \rangle = \frac{1}{R} \sum_{k=1}^{R} X_k, \tag{44}$$

$$\sigma^2(X) = \frac{1}{R-1} \sum_{k=1}^{R} (X_k - \langle X \rangle)^2, \tag{45}$$

$$\mathrm{CV}(X) = \frac{\sigma(X)}{\langle X \rangle}. \tag{46}$$

Given a time dependent quantity $x(t)$ on an interval $[0,T]$, we denote its time average by $\overline{x(t)}$, so that

$$\overline{x(t)} = \frac{1}{T} \int_0^T x(t) dt. \tag{47}$$

6.3. Verification: comparison of WFA with high resolution sectional model

To verify the WFA we compared PartMC against a high-resolution sectional solution to the Smoluchowski equation for a Brownian kernel [46]. For this test we used an ensemble of $R = 100$ PartMC runs with $N_p = 10^4$ particles, a time step of 60 s and a weighting exponent of $\alpha = -1$. This model configuration is comparable to the one used in the full urban plume scenario presented later in the paper. The sectional model was that of Bott [47], using a timestep of 1 s and 1000 logarithmically spaced sections between diameters 10^{-4} μm and 10^2 μm.

Fig. 1 shows the result of this comparison for the number size distribution (left) and the mass size distribution (right). The solid blue line is the solution for the sectional code at $t = 11$ h. To display the PartMC results we produced a size distribution for each ensemble member using 100 logarithmic bins between 10^{-4} μm and 10^2 μm, and calculated the average size distribution and the corresponding standard deviation over all ensemble members. Note that the use of size bins was only introduced in post-processing for calculating and plotting the size distributions. The errorbars are the 95% confidence intervals for the mean per size bin. We see that the PartMC solution agrees well with the high-resolution sectional solution.

We also investigated the relative magnitude of the time-discretization error compared to the error that arises as a result from a finite ensemble size, as shown in Fig. 2. We computed the expected L^2-norm of the mean number-and mass-distribution errors compared to the same high-resolution sectional solution as for Fig. 1, using the same simulation parameters for the base case (blue line), i.e. a weighting exponent of $\alpha = -1$ and $N_p = 10^4$ computational particles. The mean distribution was estimated using 100 trials and a variable ensemble size R. The dotted lines are the corresponding 95% confidence intervals.

For the two top panels in Fig. 2 this was repeated for different timestep sizes, ranging from $\Delta t = 1$ s to $\Delta t = 3600$ s. The results demonstrate the balance between time-discretization error and finite-ensemble error. For small ensemble sizes the

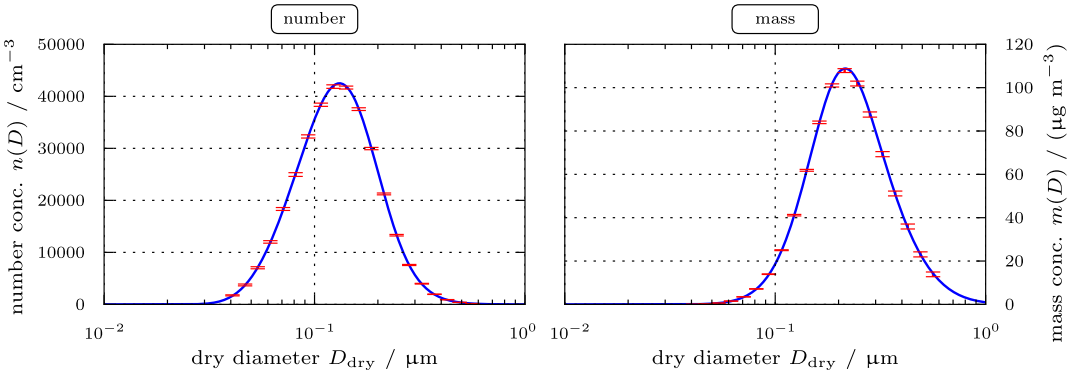

Fig. 1. Comparison of PartMC using WFA against a high resolution sectional solution to the Smoluchowski equation for a Brownian kernel. The blue solid line is the solution for the sectional code at $t = 11$ h. The red errorbars are the 95% confidence intervals for the mean resulting from an ensemble of 100 PartMC runs. All runs used a weighting exponent of $\alpha = -1$ and $N_p = 10^4$ computational particles. (For interpretation of the references to colour in this figure legend, the reader is referred to the web version of this article.)

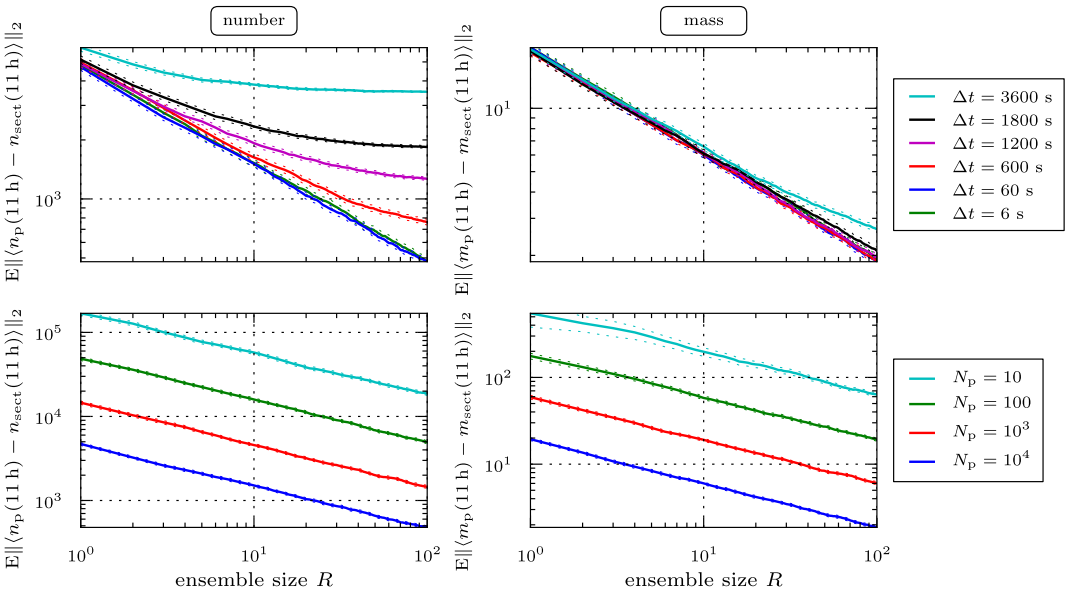

Fig. 2. Expected L^2-norm of the mean number (left) and mass (right) distribution errors as a function of the ensemble size. All runs used a weighting exponent of $\alpha = -1$. The expected value was estimated with 100 trials and the dotted lines are the corresponding 95% confidence intervals. For the top panels the number of computational particles was $N_\mathrm{p} = 10^4$ and the timestep Δt varied. For the bottom panels the timestep was $\Delta t = 60$ s and the number of computational particles N_p varied. We see that for timesteps of $\Delta t = 60$ s or less and any number of computational particles N_p, the error is dominated by the finite-ensemble error.

finite-ensemble error dominates, whereas for large ensemble sizes the total error cannot fall below the time-discretization error. We see that for a timestep of $\Delta t = 60$ s or less, the time discretization error is sufficiently small that it is negligible compared to the finite-ensemble error for ensembles of up to $R = 100$ members. As all later simulations in this paper used an ensemble of size $R = 100$ and a timestep of $\Delta t = 60$ s, we believe that the effect of time-discretization on the results is insignificant. For the two bottom panels in Fig. 2 the number of computational particles N_p was varied, ranging from $N_\mathrm{p} = 10$ to $N_\mathrm{p} = 10^4$. The time step in these cases was always $\Delta t = 60$ s. For these cases the finite-ensemble error always dominates the time-discretization error.

6.4. Setup of case study

In this section we describe the results from the application of PartMC-MOSAIC with the WFA described in Section 5 to a scenario relevant for atmospheric conditions. We carried out a series of simulations with PartMC-MOSAIC based on the urban plume scenario described in Zaveri et al. [11]. To quantify the performance of the WFA, we compared the output of a suite of ensemble runs. We performed ensemble runs with 10^3, 10^4, and 10^5 initial computational particles. Moreover we repeated each of these for six different weighting functions $W(D) = (D/D_0)^\alpha$ for $\alpha = +1, 0, -1, -2, -3, -4$ (see Eq. (4)). Each ensemble comprised $R = 100$ realizations.

The main features of the PartMC-MOSAIC model are briefly described here. A detailed description is given in Riemer et al. [14] and Zaveri et al. [11]. The Particle Monte Carlo model, PartMC, explicitly resolves and tracks the composition of many individual aerosol particles within a well-mixed computational volume. Emissions of primary aerosol particles into the computational volume, vertical entrainment and dilution with background air, and Brownian coagulation processes are simulated stochastically in PartMC.

PartMC is coupled with the state-of-the-art aerosol chemistry model MOSAIC (Model for Simulating Aerosol Interactions and Chemistry), which is described in detail in Zaveri et al. [2]. MOSAIC includes deterministic treatments for gas-phase photochemistry Zaveri and Peters [48], particle phase thermodynamics [49,50], and fully dynamic (kinetic) gas-particle mass transfer [2]. MOSAIC treats key aerosol species including sulfate (SO_4), nitrate (NO_3), chloride (Cl), carbonate (CO_3), methanesulfonic acid (MSA), ammonium (NH_4), sodium (Na), calcium (Ca), other inorganic mass (OIN), black carbon (BC), primary organic aerosol (POA), and secondary organic aerosol (SOA). OIN includes species such as SiO_2, metal oxides, and other unmeasured or unknown inorganic species present in aerosols. All particles are assumed to be spherical. The coupled model system, PartMC-MOSAIC, predicts number, mass, and full composition distributions on a particle-by-particle basis.

As in Zaveri et al. [11], we simulated the development of a particle population in a Lagrangian air parcel over the course of several hours, in our case 24 hours. The simulation started at 06:00 local standard time (LST). It initially contained background air, which was assumed to be composed of 50 ppbv O_3 and low levels of other trace gases along with an

Table 1
Initial and emitted aerosol distribution parameters. The initial aerosol distribution is also used as the background aerosol distribution. The percentages for the composition are by mass. E is the area source strength of particle emissions. Dividing E by the mixing height and multiplying by a normalized composition distribution gives the number distribution emission rate.

Initial/background	N/m^{-3}	D_{gn}/μm	σ_g	Composition by mass
Aitken mode	$1.8 \cdot 10^9$	0.02	1.45	49.6% $(NH_4)_2SO_4$, 49.6% SOA + 0.8% BC
Accumulation mode	$1.5 \cdot 10^9$	0.116	1.65	49.6% $(NH_4)_2SO_4$, 49.6% SOA + 0.8% BC
Emissions	E/(m^{-2} s^{-1})	D_{gn}/μm	σ_g	Composition by mass
Meat cooking	$9 \cdot 10^6$	0.086	1.9	100% POA
Diesel vehicles	$1.6 \cdot 10^8$	0.05	1.7	30% POA, 70% BC
Gasoline vehicles	$5 \cdot 10^7$	0.05	1.7	80% POA, 20% BC

internally-mixed ammonium sulfate and secondary organic aerosol with trace amounts of black carbon such that the single scattering albedo was about 0.97. This value is typical for rural, relatively unpolluted areas [51,52].

We assume that during the first 12 hours of simulation the parcel was advected over a large urban area, and it therefore experienced continuous emissions of NO_x, SO_2, CO, volatile organic compounds (VOCs), and primary aerosol particles of three different types diesel soot (70% BC + 30% POA), gasoline soot (20% BC + 80% POA), and meat cooking primary organic aerosol (100% POA), see Table 1 for detailed information. The air parcel also experienced dilution due to vertical entrainment of background air during the first 6 h as the mixed-layer continued to grow. In addition, and at all times, it experienced dilution with background air due to horizontal dispersion, which was modeled as a first order process, assuming a rate of 5.4% h^{-1}.

Note that the number of computational particles in the simulation changed over time as particles were added by emissions and dilution and removed by coagulation and dilution. To maintain adequate statistics while avoiding computational

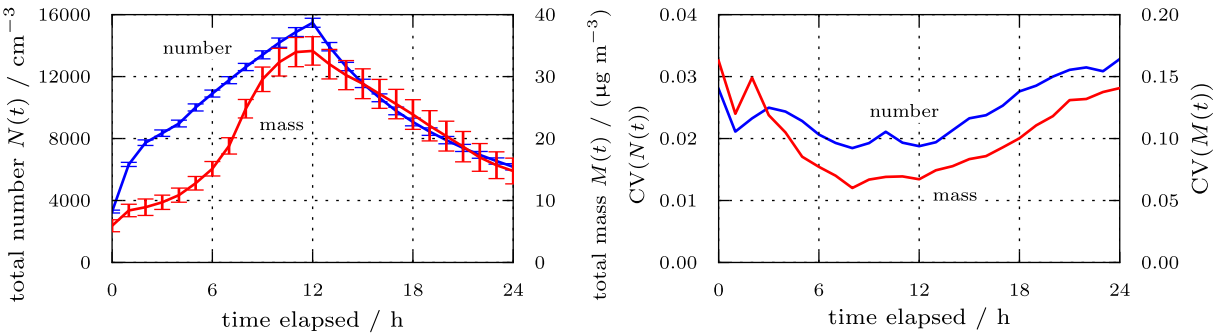

Fig. 3. Left: time evolution of the ensemble averages of total number concentration $\langle N(t)\rangle$ and total mass concentration $\langle M(t)\rangle$. The weighting exponent is $\alpha = 0$, and the initial number of computational particles is $N_p(0) = 10^3$. The errorbars represent the standard deviations $\sigma(N(t))$ and $\sigma(M(t))$. Recall that in this simulation, particles are emitted for the first twelve hours, which leads to the growth over the first half of both particle number and mass. Right: corresponding coefficients of variation CV($N(t)$) and CV($M(t)$), respectively.

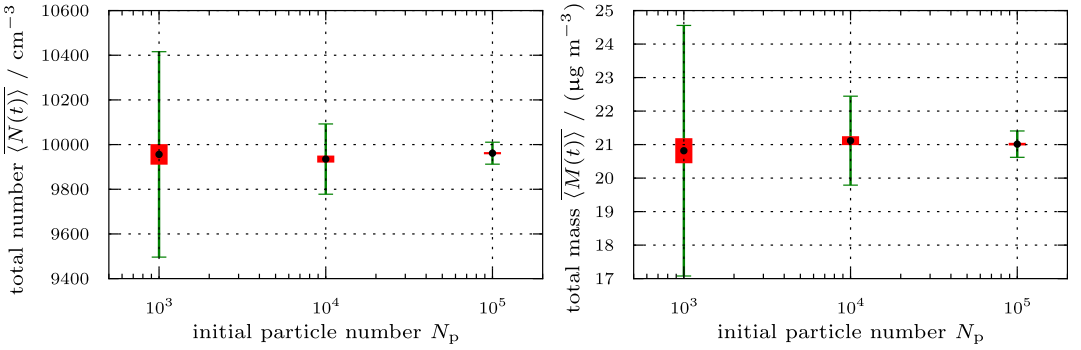

Fig. 4. Left: time average of ensemble averaged total number concentration $\overline{\langle N(t)\rangle}$. Right: time average of ensemble averaged total mass concentration $\overline{\langle M(t)\rangle}$. The weighting exponent is $\alpha = 0$. In red, we have plotted a range of size $\frac{1}{\sqrt{R}} t_{95\%,R-1} \overline{\sigma(N(t;N_{p_1}))}$, which is the 95% confidence interval for the mean. The green errorbars represent the range in which we would expect 95% of the samples to lie, i.e. the range with width $t_{95\%,R-1}\overline{\sigma(N(t;N_{p_1}))}$ and center given by the sample mean. (For interpretation of the references to colour in this figure legend, the reader is referred to the web version of this article.)

limits, we occasionally adjust the particle number. Whenever the number of particles becomes less than half of the original particle number we double the computational volume and double the number of particles by duplicating each particle. Whenever we have more than twice the original number of particles we halve the computational volume and discard half of the particles, chosen at random.

6.5. Bulk quantities

Fig. 3 (left) shows the evolution of the ensemble-averaged total number concentration $\langle N(t)\rangle$ and the total mass concentration $\langle M(t)\rangle$ for the simulation with $\alpha = 0$ and $N_p = 10^3$. The errorbars indicate the standard deviations $\sigma(N(t))$ and $\sigma(M(t))$, respectively. The total number concentration $\langle N(t)\rangle$ increased during the first 12 h of simulation owing to the continuous particle emissions. After emissions were turned off, $\langle N(t)\rangle$ decreased as a result of dilution with the background and coagulation. The increase of total mass concentration $\langle M(t)\rangle$ is partly due to particle emissions and partly due to the formation of secondary species such as ammonium nitrate, ammonium sulfate and SOA. In the second part of the simulation $\langle M(t)\rangle$ decreased because of dilution.

From Fig. 3 (left) we see that the bulk quantities $\langle N(t)\rangle$ and $\langle M(t)\rangle$ show a pronounced dependence on time due to the underlying emission pattern, photochemistry, coagulation, and dilution. The coefficients of variation, shown in Fig. 3 (right) CV($N(t)$) and CV($M(t)$) also vary with time, however much less than the corresponding bulk quantities. To simplify the discussion we average the hourly values of these quantities over the whole simulation period.

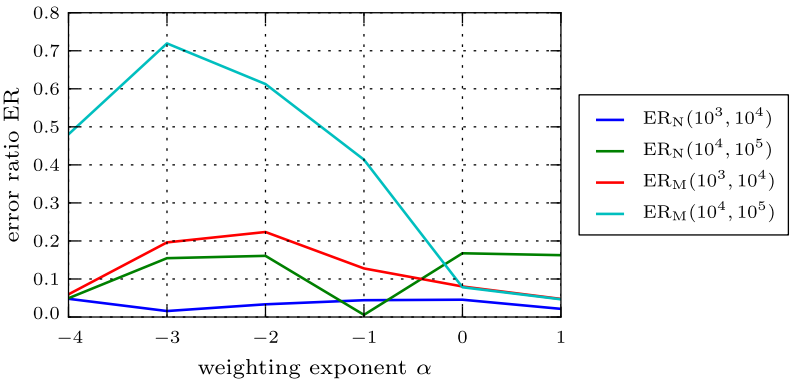

Fig. 5. Error ratios for number, $\mathrm{ER_N}$, and error ratios for mass, $\mathrm{ER_M}$, as a function of weighting exponent α. The fact that this ratio is always less than one, and in many cases significantly so, emphasizes that the sample error per realization dominates the errors in mean incurred from using finite-size populations.

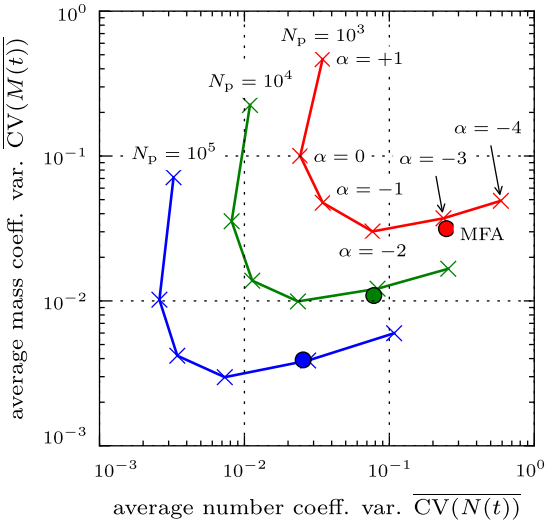

Fig. 6. Coefficients of variation for mass, $\overline{\mathrm{CV}(M(t))}$, versus coefficients of variation for number $\overline{\mathrm{CV}(N(t))}$ for simulations with 10^3,10^4, and 10^5 initial particles N_p and different values for the weighting exponent α. The filled circles indicate the results using MFA.

Fig. 4 illustrates how the time-and ensemble-averaged number and mass concentrations shown in Fig. 3, $\overline{\langle N(t)\rangle}$ and $\overline{\langle M(t)\rangle}$, compare as the initial particle number N_p varies. The length of the red bar indicates the 95% confidence interval for the mean, using Student's t-test for statistical significance. In green are the 95% confidence intervals per sample.

From this figure we conclude that the statistical error is larger than the discretization error that results from using a finite number of particles to represent the population. This justifies our choice of ensemble size and demonstrates that the numbers of initial particles, N_p, are large enough. Fig. 5 confirms that this is true for all weighting exponents α used here. Here we show the error ratios ER for number and mass, respectively, as a function of weighting exponent α. We define the error ratio for number, $\mathrm{ER_N}$, as

$$\mathrm{ER_N}(N_{p_1}, N_{p_2}) = \frac{|\overline{\langle N(t;N_{p_2})\rangle} - \overline{\langle N(t;N_{p_1})\rangle}|}{t_{95\%,R-1}\overline{\sigma(N(t;N_{p_1}))}} = \frac{|\overline{\langle N(t;N_{p_2}) - N(t;N_{p_1})\rangle}|}{t_{95\%,R-1}\overline{\sigma(N(t;N_{p_1}))}}, \tag{48}$$

where $t_{95\%,R-1}$ is the 95% percentile for Student's t-distribution with $R-1$ degrees of freedom, and we will take (N_{p_1}, N_{p_2}) to be either $(10^3, 10^4)$ or $(10^4, 10^5)$. The error ratio $\mathrm{ER_M}(N_{p_1}, N_{p_2})$ for mass is defined analogously. As Fig. 5 shows, $\mathrm{ER_N}$ and $\mathrm{ER_M}$ are always smaller than 1, confirming the statement above that for our simulations the difference in the sample mean for different N_p is small compared to the sample standard deviation. Fig. 6 summarizes the trade off in magnitude of coefficient of variation with respect to number and with respect to mass as the weighting exponents α and the number of initial particles N_p vary. From this plot we can make the following conclusions: For a given α, the larger N_p the smaller is $\overline{\mathrm{CV}(N(t))}$ and $\overline{\mathrm{CV}(M(t))}$. The shape of the curves for N_p = const suggests that $\alpha > 0$ and $\alpha < -2$ should not be used. Moving from $\alpha = 0$ to -1 and -2 reduces $\overline{\mathrm{CV}(M(t))}$ at the expense of $\overline{\mathrm{CV}(N(t))}$. Furthermore we see that the same $\overline{\mathrm{CV}(M(t))}$ value that is achieved with the $N_p = 10^5$ simulation can be achieved with the $N_p = 10^4$ simulation using a weighting of $\alpha = -2$. However in doing so,

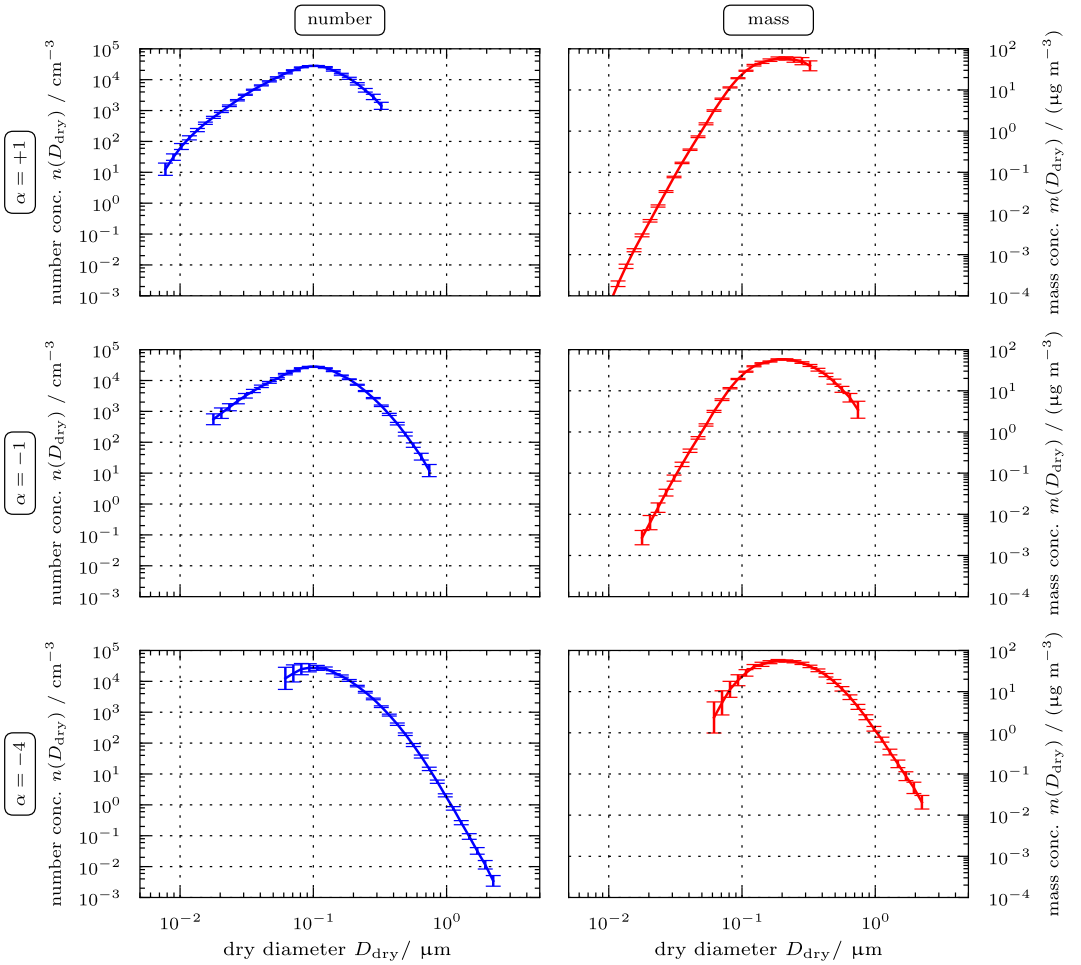

Fig. 7. Ensemble averages of one-dimensional size distributions for initial number of particles $N_p = 10^4$, $t_0 = 11$ h, and different weighting exponents. Left: distributions of number concentration $\langle n(D_{dry})\rangle$. Right: distributions of dry mass concentration $\langle m(D_{dry})\rangle$. Top: $\alpha = 1$, middle: $\alpha = -1$, bottom: $\alpha = -4$.

$\overline{\mathrm{CV}(N(t))}$ increases by a factor of 9. Also marked in Fig. 6 are the values that result when using the MFA algorithm, which gives results very close to the simulations with $\alpha = -3$ as expected.

6.6. One-dimensional aerosol size distributions

Fig. 7 shows the results for the one-dimensional size distributions at $t = 11$ h. The initial particle number was $N_p = 10^4$ in all cases. The left column depicts the ensemble averages of the number concentrations, $\langle n(D_{dry})\rangle$ for $\alpha = 1$, $\alpha = -1$, and $\alpha = -4$, from top to bottom. The right column shows the corresponding mass concentrations $\langle m(D_{dry})\rangle$. The errorbars are the standard deviations per bin, $\sigma(n(D_{dry}))$ and $\sigma(m(D_{dry}))$. Recall that the use of size bins was only introduced in post-processing for calculating and plotting the size distributions.

The number size distribution at $t = 11$ h is unimodal and shows a maximum for $D_{dry} = 0.1$ μm. This maximum is a result of the continued emissions and subsequent growth from condensation of secondary species, mainly ammonium nitrate. As expected $\sigma(n(D_{dry}))$ and $\sigma(m(D_{dry}))$ increase in magnitude towards the edges of the spectra. The comparison of the figures for the three different weighting exponents shows how the choice of α influences the representation of the size distribution. The smaller α, the more weight is given to larger particles, and hence the right-hand side of the spectrum is better resolved. This is associated with a loss of resolution at the small sizes. While for $\alpha = 1$ the size distribution is resolved from about 8 nm to

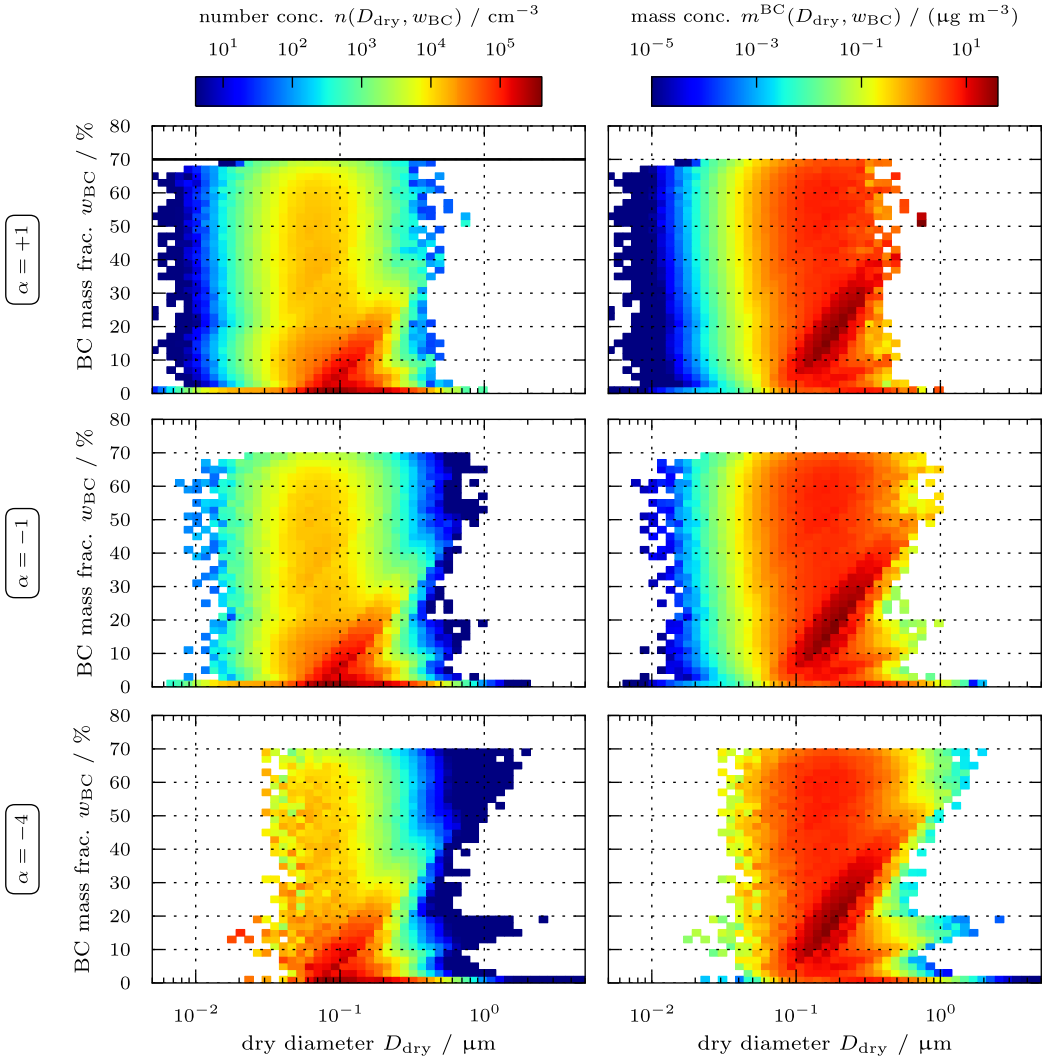

Fig. 8. Left: ensemble averages of two-dimensional number size distributions $\langle n(D, w_{BC})\rangle$ at $t_0 = 11$ h. Right: ensemble averages of two-dimensional BC mass size distributions $\langle m^{BC}(D, w_{BC})\rangle$ at $t_0 = 11$ h. Top: $\alpha = 1$, middle: $\alpha = -1$, bottom: $\alpha = -4$. The initial number of particles was $N_p = 10^4$ in all cases.

320 nm, for $\alpha = -4$ this interval has shifted up to 62 nm to 2200 nm. Using a smaller number of computational particles N_p narrows this range and increases $\sigma(n(D_{dry}))$ and $\sigma(m(D_{dry}))$ (not shown).

6.7. Black carbon mixing state and CCN activity

Having explored the WFA performance for the bulk quantities as well as for the one-dimensional aerosol size distributions, we now move on to investigating the results for certain two-dimensional size distributions of physical relevance. Here we focus on two target quantities, first the black carbon mixing state and secondly the number of cloud condensation nuclei that would activate at a pre-defined environmental supersaturation.

Fig. 8 shows ensemble averages of the two-dimensional size distributions for number concentration, $\langle n(D, w_{BC})\rangle$ and BC mass concentration, $\langle m^{BC}(D, w_{BC})\rangle$, for the same point in time and for the same values of α as in Fig. 7. The horizontal black line at $w_{BC} = 70\%$ shows the maximum black carbon fraction that particles can have in our scenario. At $t = 11$ h the mixing state of the particles with respect to BC has evolved into a continuum between $w_{BC} = 0\%$ and $w_{BC} = 70\%$. While fresh emissions can contain up to 70% BC (diesel soot particles), most of the particles by number have been heavily aged after 11 h of simulation and contain less than 20% BC as a result of condensation of secondary species and coagulation. Overall, the same features of the size distributions are apparent for all three different weighting factors. However, the resolved size range varies strongly with α as has already been seen in Fig. 7.

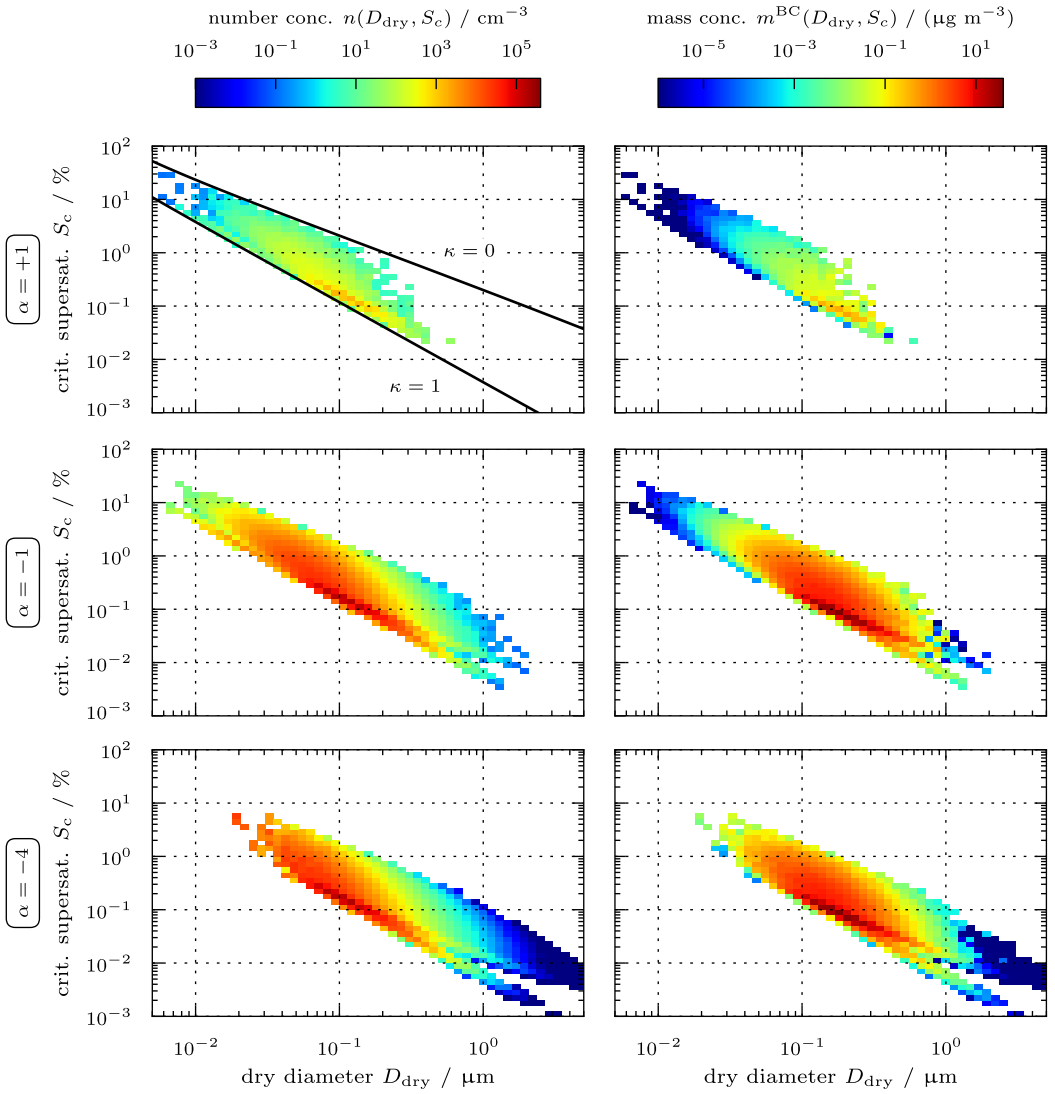

Fig. 9. Left: ensemble averages of two-dimensional number size distributions $\langle n(D,S_c)\rangle$ at $t_0 = 11$ h. Right: ensemble averages of two-dimensional BC mass size distributions $\langle m^{BC}(D,S_c)\rangle$. Top: $\alpha = 1$, middle: $\alpha = -1$, bottom: $\alpha = -4$. The initial number of particles was $N_p = 10^4$ in all cases. The two black lines in the upper left panel show the relationship for two extreme values of the hygroscopicity parameter κ.

Given that we track the composition evolution of each individual particle throughout the simulation, we can calculate the critical supersaturation $S_c(\boldsymbol{\mu})$ that is required to activate a particle. We do this as described in Riemer et al. [53] (see Eqs. (3)–(8) therein).

Two-dimensional size distributions $\langle n(D_{dry},S_c)\rangle$ and $\langle m^{BC}(D_{dry},S_c)\rangle$ are shown in Fig. 9 for the same parameters as in Fig. 8. The differences in mixing state at a certain particle size translate into a distribution of critical supersaturations at that size, e.g. for 100 nm particles at $t = 11$ h the critical supersaturations ranged between 0.1% and 1.2%. The two black lines in the upper left panel show the relationship for two extreme values of the hygroscopicity parameter κ, $\kappa = 1$ (very hygroscopic) and $\kappa = 0$ (very non-hygroscopic). We see that the particle distributions in our simulations span the range between these extremes. As in Fig. 8, the same features of the size distributions are apparent for all three different weighting factors, but the resolved size range varies strongly with α. This has consequences for the total number of CCN at a given environmental supersaturation S_{env}, $N_{CCN}(S_{env})$, defined as:

$$N_{CCN}(S_{env}) = \int_{-\infty}^{\infty}\int_{-\infty}^{\log_{10}S_{env}} n(D_{dry},S_c)d\log_{10}S_c d\log_{10}D_{dry}. \tag{49}$$

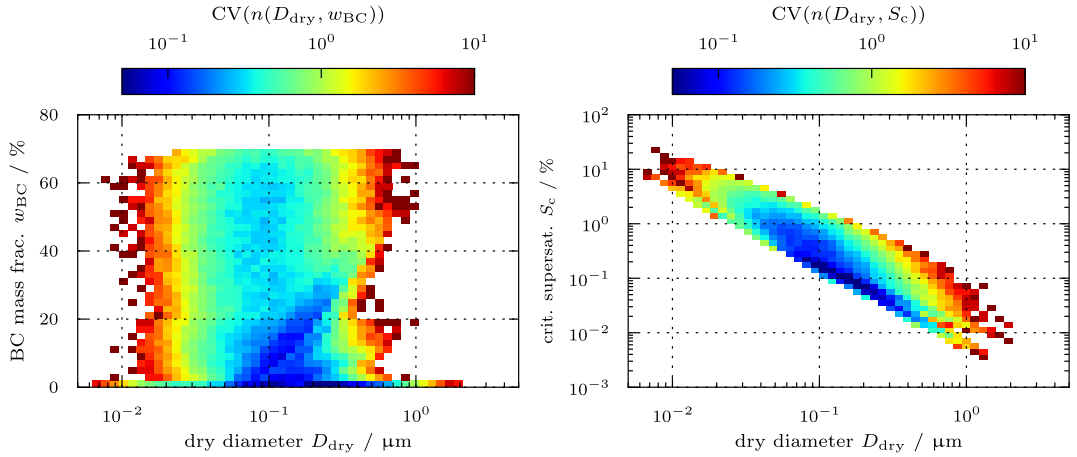

Fig. 10. Two-dimensional distributions of the coefficient of variations for initial number of particles $N_p = 10^4$, time $t_0 = 11$ h, and weighting exponent $\alpha = -1$. Left: coefficient of variation for the two-dimensional number distribution $n(D,w_{BC})$, CV($n(D,w_{BC})$). Right: coefficient of variation for the two-dimensional number distribution $n(D,S_c)$, CV($n(D,S_c)$).

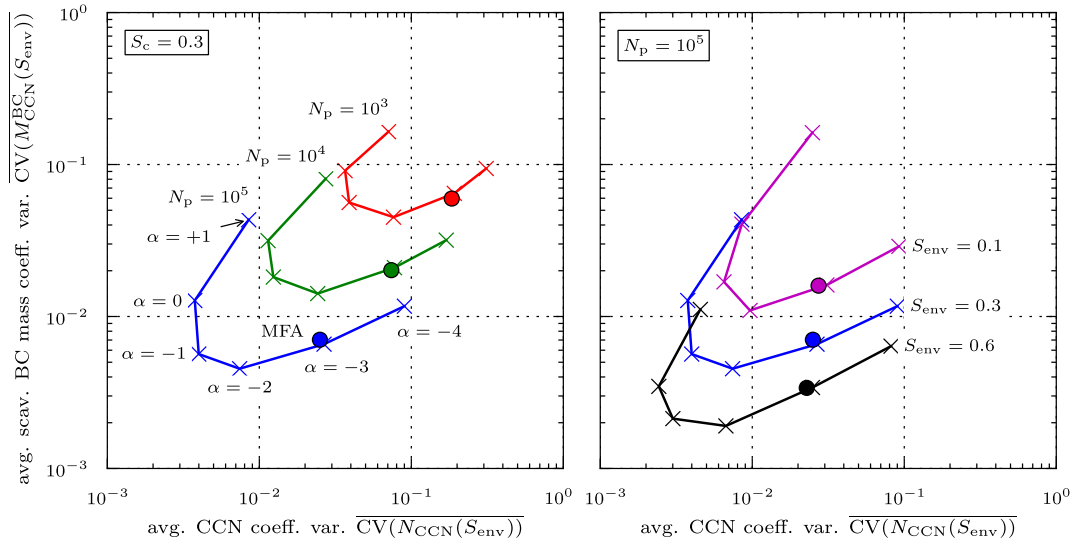

Fig. 11. Coefficients of variation for scavenged BC mass, $\overline{\mathrm{CV}(M^{BC}_{CCN}(S_{env}))}$ versus coefficients of variation for CCN $\overline{\mathrm{CV}(N_{CCN}(S_{env}))}$ for different weighting exponents α. Left: the environmental supersaturation is $S_{env} = 0.3\%$. The initial number of particles N_p is 10^3, 10^4, and 10^5 particles. Right: the initial number of particles is $N_p = 10^5$, and the supersaturation threshold varies. The filled circles indicate the results using MFA.

For low values of S_{env} the total number of CCN will be underestimated if the right-hand side of the spectrum is underresolved as it is the case for example for $\alpha = 1$. A similar argument applies to the mass of black carbon, $M^{BC}_{CCN}(S_{env})$ that is associated with these CCN:

$$M^{BC}_{CCN}(S_{env}) = \int_{-\infty}^{\infty} \int_{-\infty}^{\log_{10} S_{env}} m^{BC}(D_{dry}, S_c) d\log_{10} S_c d\log_{10} D_{dry}. \tag{50}$$

We will come back to this issue for the discussion of Fig. 11. Fig. 10 shows the two-dimensional distributions of the coefficients of variation, $CV(n(D,w_{BC}))$ and $CV(n(D,S_c))$ corresponding to Figs. 8 and 9. For brevity we only include the case for $\alpha = -1$. The coefficients of variation range between 0.0344 and 9.95 with the higher values at the edges of the distributions.

Analogously to Figs. 6, 11 summarizes the trade off in magnitude of the coefficient of variation with respect two quantities of interest, in this case $N_{CCN}(S_{env})$ and $M^{BC}_{CCN}(S_{env})$ defined in Eqs. (49) and (50) as the weighting exponents α and the number of initial particles N_p vary. We chose three different supersaturation thresholds, $S_{env} = 0.1\%, 0.3\%, 0.6\%$. This range is consistent with the highly polluted conditions of the urban plume scenario given a typical range of updraft velocities from 0.2–0.5 ms^{-1} (stratus clouds) to 2–5 ms^{-1} (convective clouds).

Fig. 11 (left) shows the dependence on initial particle number N_p for $S_{env} = 0.1\%$. The filled circles were added to show the results using MFA. The result is qualitative similar to Fig. 6, i.e. the coefficients of variation decreased as N_p increased. $\overline{CV(M^{BC}_{CCN}(S_{env}))}$ was lowest for $\alpha = -2$, whereas $\overline{CV(N_{CCN}(S_{env}))}$ was lowest for $\alpha = -1$.

In Fig. 11 (right) the initial particle number was $N_p = 10^5$, and the dependence on supersaturation threshold S_{env} is shown. The largest values of the coefficients of variation are obtained for small values of S_{env}.

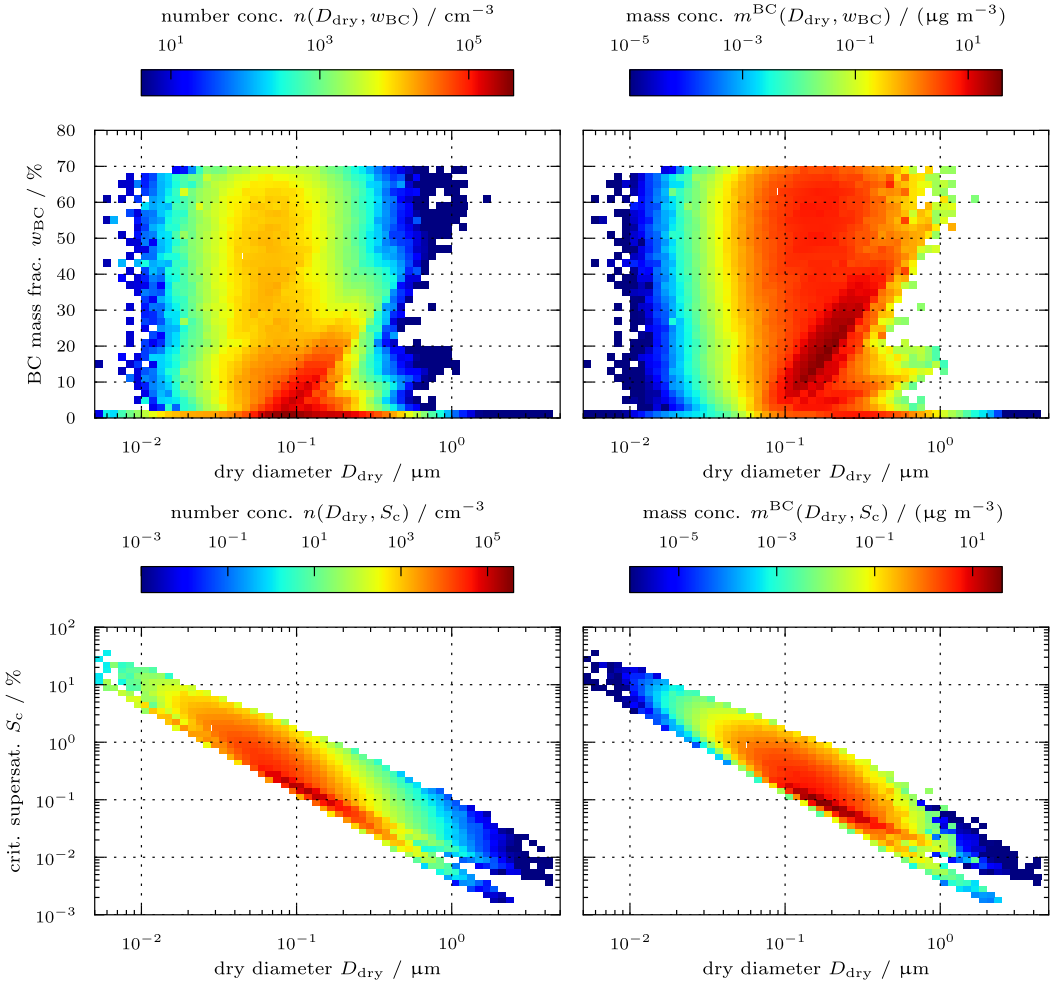

Fig. 12. Composites of two-dimensional distributions for initial number of particles $N_p = 10^3$, $t_0 = 11$ h. Top: $n(D,w_{BC})$ and $m^{BC}(D,w_{BC})$. Bottom: $n(D,S_c)$ and $m^{BC}(D,S_c)$.

Having the particle-resolved results for the six different weighting functions available, we can create composite distributions for all the size distributions that we have shown so far. That is, we have independent ensemble averages $\langle X_\alpha \rangle$ of a quantity X, for different values of α. We will take a weighted linear combination of the $\langle X_\alpha \rangle$ as a composite estimate $\langle X_{\text{comp}} \rangle = \sum_\alpha (\delta_a / \delta_{\text{tot}}) \langle X_\alpha \rangle$ of X, and we should choose a weighting that prefers the more reliable estimates $\langle X_\alpha \rangle$. As is well known, when combining random quantities with different variances, the least-variance linear combination of these quantities is the one which weights inversely to the variance of each quantity. Of course, we do not have access to these variances and must choose an estimator from the observed quantities. Under the assumption that the ensemble samples come from a Poisson distribution with the correct mean, the ensemble mean is a convergent unbiased estimator to this variance. Of course, the sample ensemble variance is also a convergent unbiased estimator to this variance, but the former is more effective for small ensemble sizes. Thus in the aggregate computation, we weight $\langle X_\alpha \rangle$ proportionally to the ensemble average of the number of computational particles $\langle N_\alpha \rangle$:

$$\gamma_\alpha = \langle N_\alpha \rangle, \tag{51}$$

$$\gamma_{\text{tot}} = \sum_{\alpha=-4}^{\alpha=1} \gamma_\alpha, \tag{52}$$

$$\langle X_{\text{comp}} \rangle = \sum_{\alpha=-4}^{\alpha=1} \frac{\gamma_\alpha}{\gamma_{\text{tot}}} \langle X_\alpha \rangle. \tag{53}$$

All of the above quantities are computed per size and composition bin, so the composite distribution will depend more on the $\alpha = +1$ estimate at small diameters, and more on the $\alpha = -4$ estimate at large diameters, with the other α estimates used appropriately.

A set of composite figures is shown in Fig. 12 where the initial number of particles was $N_p = 10^3$. Compare this to Figs. 8 and 9, which were obtained with an initial particle number $N_p = 10^4$. One can see that the composite figures with $N_p = 10^3$ resolve well across more scales than any of the $N_p = 10^4$ figures.

7. Conclusions

In this paper we describe the development and application of the Weighted Flow Algorithms (WFA) for particle-resolved methods, a generalized way of weighting computational particles to improve efficiency. We have shown that there exist particle methods which work for any given weighting function and how different weighting functions are appropriate for measuring different observables. In particular, for the application shown in this paper, we used weighting functions that are power laws in particle size. We derived the particle evolution equations taking into account coagulation and particle growth and showed how this relates to the Mass Flow Algorithm of Babovsky [20] and Eibeck and Wagner [21–25].

We quantified the performance of using different weighting functions by applying the WFA to PartMC-MOSAIC using the urban plume scenario described in Zaveri et al. [11] where we simulated the evolution of the mixings state of an aerosol population in a polluted environment undergoing emission, dilution, coagulation and particle growth over the course of 24 h. We repeated the simulation for different numbers of initial computational particles and for different weighting exponents and calculated coefficients of variation for various quantities. Here we focused on total number concentration and total mass concentration as well as two quantities that are important for aerosol-cloud interactions, i.e. the number of cloud condensation nuclei and the mass of associated black carbon given a certain environmental supersaturation. To minimize the coefficients of variation for both number-and mass-based quantities we found that $\alpha > 0$ and $\alpha < -2$ should not be used. Moving from $\alpha = 0$ to -1 and -2 reduces the coefficient of variation for the mass-based quantities at the expense of the number-based quantities. We also developed collated data sets which used the most reliable data from each of the weighted simulation, producing particle size distributions with the same accuracy but using fewer particles.

Acknowledgments

The authors acknowledge funding from the National Science Foundation (NSF) under Grant CMG-0934491.

Appendix A. General asymmetric coagulation algorithms

In this section, we generalize the method used in Step 3 of Section 4.1 to the most general splitting method and show: (1) our algorithm and the MFA are both special cases of this general framework and (2) a choice of algorithm of MFA-type can only work for a mass-weighted scheme and cannot be generalized to other weights.

In particular, we will describe a family of different schemes which are all designed to give the same mean and which will all converge to the correct answer as $N_p \to \infty$. However, these different schemes might have different variances and in certain computational scenarios some might be preferable to another. As we see in Figs. 6 and 11, however, we see that the "independent" scheme we describe in Section 4 and the MFA scheme give a similar variance. In other specific computational scenarios, however, one of these schemes might be preferable to another.

As before, we assume that we have only pairwise interactions and that these interactions are "coagulation-like", i.e. all events correspond to particles $\boldsymbol{\mu}$ and $\boldsymbol{\nu}$ combining to form particle $\boldsymbol{\mu}+\boldsymbol{\nu}$. We consider any two-stage method of the following form: first, the triplet $(\boldsymbol{\mu},\boldsymbol{\nu},\boldsymbol{\mu}+\boldsymbol{\nu})$ is chosen with some rate; second, after the triplet has been chosen we choose the event involving this triplet with some probability. Specifically, we denote the rate of choosing the triplet by $T(\boldsymbol{\mu},\boldsymbol{\nu})$ and then choose the eight probabilities $p_{ijk}(\boldsymbol{\mu},\boldsymbol{\nu})$ for $i,j,k\in\{0,1\}$. The indexes i,j,k correspond to the existence of particles $\boldsymbol{\mu}$, $\boldsymbol{\nu}$, and $\boldsymbol{\mu}+\boldsymbol{\nu}$ after the event, with 1 indicating that the corresponding particle is present and 0 that it is not. The eight probabilities thus correspond to the probabilities of the transitions:

$$p_{000}:(\boldsymbol{\mu},\boldsymbol{\nu})\mapsto(), \tag{A.1a}$$
$$p_{001}:(\boldsymbol{\mu},\boldsymbol{\nu})\mapsto(\boldsymbol{\mu}+\boldsymbol{\nu}), \tag{A.1b}$$
$$p_{010}:(\boldsymbol{\mu},\boldsymbol{\nu})\mapsto(\boldsymbol{\nu}), \tag{A.1c}$$
$$p_{011}:(\boldsymbol{\mu},\boldsymbol{\nu})\mapsto(\boldsymbol{\nu},\boldsymbol{\mu}+\boldsymbol{\nu}), \tag{A.1d}$$
$$p_{100}:(\boldsymbol{\mu},\boldsymbol{\nu})\mapsto(\boldsymbol{\mu}), \tag{A.1e}$$
$$p_{101}:(\boldsymbol{\mu},\boldsymbol{\nu})\mapsto(\boldsymbol{\mu},\boldsymbol{\mu}+\boldsymbol{\nu}), \tag{A.1f}$$
$$p_{110}:(\boldsymbol{\mu},\boldsymbol{\nu})\mapsto(\boldsymbol{\mu},\boldsymbol{\nu}), \tag{A.1g}$$
$$p_{111}:(\boldsymbol{\mu},\boldsymbol{\nu})\mapsto(\boldsymbol{\mu},\boldsymbol{\nu},\boldsymbol{\mu}+\boldsymbol{\nu}). \tag{A.1h}$$

We will find it convenient to use the notation

$$p_{ijX}(\boldsymbol{\mu},\boldsymbol{\nu})=\sum_{k\in\{0,1\}}p_{ijk}(\boldsymbol{\mu},\boldsymbol{\nu}),$$
$$p_{iXX}(\boldsymbol{\mu},\boldsymbol{\nu})=\sum_{j\in\{0,1\}}\sum_{k\in\{0,1\}}p_{ijk}(\boldsymbol{\mu},\boldsymbol{\nu})$$

and similarly. Note that we have:

$$0\leqslant p_{ijk}(\boldsymbol{\mu},\boldsymbol{\nu})\leqslant 1, \tag{A.2}$$
$$p_{XXX}(\boldsymbol{\mu},\boldsymbol{\nu})=1. \tag{A.3}$$

The large-N limit for c is:

$$\frac{\partial c(\boldsymbol{\mu})}{\partial t}=\frac{1}{2}\int_{[\mathbf{0},\boldsymbol{\mu}]}(T(\boldsymbol{\nu},\boldsymbol{\mu}-\boldsymbol{\nu})p_{XX1}(\boldsymbol{\nu},\boldsymbol{\mu}-\boldsymbol{\nu})+T(\boldsymbol{\mu}-\boldsymbol{\nu},\boldsymbol{\nu})p_{XX1}(\boldsymbol{\mu}-\boldsymbol{\nu},\boldsymbol{\nu}))c(\boldsymbol{\nu})c(\boldsymbol{\mu}-\boldsymbol{\nu})d\boldsymbol{\nu}-\int_{[\mathbf{0},\infty]}(T(\boldsymbol{\nu},\boldsymbol{\mu})p_{X0X}(\boldsymbol{\nu},\boldsymbol{\mu})$$
$$+T(\boldsymbol{\mu},\boldsymbol{\nu})p_{0XX}(\boldsymbol{\mu},\boldsymbol{\nu}))c(\boldsymbol{\nu})c(\boldsymbol{\mu})d\boldsymbol{\nu}. \tag{A.4}$$

Since we want (A.4) to be consistent with (7), we are required to choose

$$T(\boldsymbol{\mu},\boldsymbol{\nu})p_{XX1}(\boldsymbol{\mu},\boldsymbol{\nu})+T(\boldsymbol{\nu},\boldsymbol{\mu})p_{XX1}(\boldsymbol{\nu},\boldsymbol{\mu})=K(\boldsymbol{\mu},\boldsymbol{\nu})\frac{W(\boldsymbol{\mu})W(\boldsymbol{\nu})}{W(\boldsymbol{\mu}+\boldsymbol{\nu})}, \tag{A.5a}$$
$$T(\boldsymbol{\mu},\boldsymbol{\nu})p_{0XX}(\boldsymbol{\mu},\boldsymbol{\nu})+T(\boldsymbol{\nu},\boldsymbol{\mu})p_{X0X}(\boldsymbol{\nu},\boldsymbol{\mu})=K(\boldsymbol{\mu},\boldsymbol{\nu})W(\boldsymbol{\nu}). \tag{A.5b}$$

Note that we can always symmetrize the kernel of an asymmetric method to obtain a symmetric representation of the same process. To do this, take:

$$R(\boldsymbol{\mu},\boldsymbol{\nu})=T(\boldsymbol{\mu},\boldsymbol{\nu})+T(\boldsymbol{\nu},\boldsymbol{\mu}), \tag{A.6a}$$
$$\tilde{p}_{ijk}(\boldsymbol{\mu},\boldsymbol{\nu})=\frac{T(\boldsymbol{\mu},\boldsymbol{\nu})p_{ijk}(\boldsymbol{\mu},\boldsymbol{\nu})+T(\boldsymbol{\nu},\boldsymbol{\mu})p_{jik}(\boldsymbol{\nu},\boldsymbol{\mu})}{T(\boldsymbol{\mu},\boldsymbol{\nu})+T(\boldsymbol{\nu},\boldsymbol{\mu})}. \tag{A.6b}$$

This implies:

$$R(\boldsymbol{\mu},\boldsymbol{\nu})=R(\boldsymbol{\nu},\boldsymbol{\mu}), \tag{A.7a}$$
$$\tilde{p}_{ijk}(\boldsymbol{\mu},\boldsymbol{\nu})=\tilde{p}_{jik}(\boldsymbol{\nu},\boldsymbol{\mu}). \tag{A.7b}$$

To make this algorithm optimally efficient, we want to minimize $R(\boldsymbol{\mu},\boldsymbol{\nu})$ (which, again, corresponds to having the fewest "wasted" steps in the computation). Conditions (A.5) become

$$R(\boldsymbol{\mu},\boldsymbol{\nu})\tilde{p}_{XX1}(\boldsymbol{\mu},\boldsymbol{\nu})=K(\boldsymbol{\mu},\boldsymbol{\nu})\frac{w(\boldsymbol{\mu})W(\boldsymbol{\nu})}{W(\boldsymbol{\mu}+\boldsymbol{\nu})},$$
$$R(\boldsymbol{\mu},\boldsymbol{\nu})\tilde{p}_{0XX}(\boldsymbol{\mu},\boldsymbol{\nu})=K(\boldsymbol{\mu},\boldsymbol{\nu})W(\boldsymbol{\nu}),$$

so we want to minimize $R(\boldsymbol{\mu},\boldsymbol{\nu})$ subject to

$$0\leqslant\tilde{p}_{XX1}(\boldsymbol{\mu},\boldsymbol{\nu})=\frac{K(\boldsymbol{\mu},\boldsymbol{\nu})W(\boldsymbol{\mu})W(\boldsymbol{\nu})}{R(\boldsymbol{\mu},\boldsymbol{\nu})W(\boldsymbol{\mu}+\boldsymbol{\nu})}\leqslant 1,$$
$$0\leqslant\tilde{p}_{0XX}(\boldsymbol{\mu},\boldsymbol{\nu})=\frac{K(\boldsymbol{\mu},\boldsymbol{\nu})W(\boldsymbol{\nu})}{R(\boldsymbol{\mu},\boldsymbol{\nu})}\leqslant 1,$$
$$0\leqslant\tilde{p}_{X0X}(\boldsymbol{\nu},\boldsymbol{\mu})=\frac{K(\boldsymbol{\mu},\boldsymbol{\nu})W(\boldsymbol{\mu})}{R(\boldsymbol{\mu},\boldsymbol{\nu})}\leqslant 1.$$

Therefore, an algorithm is optimal if

$$R(\boldsymbol{\mu},\boldsymbol{\nu}) = K(\boldsymbol{\mu},\boldsymbol{\nu})\frac{W(\boldsymbol{\mu})W(\boldsymbol{\nu})}{W_{\min}(\boldsymbol{\mu},\boldsymbol{\nu})} \tag{A.8a}$$

$$\tilde{p}_{X0X}(\boldsymbol{\mu},\boldsymbol{\nu}) = \frac{W_{\min}(\boldsymbol{\mu},\boldsymbol{\nu})}{W(\boldsymbol{\nu})} \tag{A.8b}$$

$$\tilde{p}_{XX1}(\boldsymbol{\mu},\boldsymbol{\nu}) = \frac{W_{\min}(\boldsymbol{\mu},\boldsymbol{\nu})}{W(\boldsymbol{\mu}+\boldsymbol{\nu})} \tag{A.8c}$$

$$W_{\min}(\boldsymbol{\mu},\boldsymbol{\nu}) = \min(W(\boldsymbol{\mu}), W(\boldsymbol{\nu}), W(\boldsymbol{\mu}+\boldsymbol{\nu})). \tag{A.8d}$$

(Note that from (A.7), we can either put the constraint on $\tilde{p}_{0XX}$ or $\tilde{p}_{X0X}$.) Compare to (12). All optimal and consistent algorithms must be chosen in this manner; however, notice that there are still many choices still free—there are seven possibilities to choose for p_{ijk} but only three constraints in (A.8). This leaves four choices free. We now show that the two algorithms described in Section 4.1 are both optimal but result from different choices made at this point.

A.1. Comparison to algorithm (12)

In the method we choose in this paper, we use *independent probabilities*, i.e. we choose the survival of any given particle independently from the others. We can choose this by taking

$$p'_{ijk}(\boldsymbol{\mu},\boldsymbol{\nu}) = p_{\text{death},i}(\boldsymbol{\nu},\boldsymbol{\mu})p_{\text{death},j}(\boldsymbol{\mu},\boldsymbol{\nu})p_{\text{birth},k}(\boldsymbol{\mu},\boldsymbol{\nu}), \tag{A.9}$$

where

$$p_{\text{death},i}(\boldsymbol{\mu},\boldsymbol{\nu}) = \begin{cases} p_{\text{death}}(\boldsymbol{\mu},\boldsymbol{\nu}) & \text{if } i=0, \\ 1-p_{\text{death}}(\boldsymbol{\mu},\boldsymbol{\nu}) & \text{if } i=1, \end{cases} \tag{A.10a}$$

$$p_{\text{birth},i}(\boldsymbol{\mu},\boldsymbol{\nu}) = \begin{cases} p_{\text{birth}}(\boldsymbol{\mu},\boldsymbol{\nu}) & \text{if } i=1, \\ 1-p_{\text{birth}}(\boldsymbol{\mu},\boldsymbol{\nu}) & \text{if } i=0 \end{cases} \tag{A.10b}$$

for

$$p_{\text{death}}(\boldsymbol{\mu},\boldsymbol{\nu}) = \tilde{p}_{X0X}(\boldsymbol{\mu},\boldsymbol{\nu}), \tag{A.11a}$$

$$p_{\text{birth}}(\boldsymbol{\mu},\boldsymbol{\nu}) = \tilde{p}_{XX1}(\boldsymbol{\mu},\boldsymbol{\nu}). \tag{A.11b}$$

This makes the removal of particles $\boldsymbol{\mu}$ and $\boldsymbol{\nu}$ and the addition of $\boldsymbol{\mu}+\boldsymbol{\nu}$ be three independent events, but with the same mean rate as the original system.

A.2. Comparison to MFA (15)

The Mass-Flow Algorithm [20–25] is given by the choices:

$$T(\boldsymbol{\mu},\boldsymbol{\nu}) = K(\boldsymbol{\mu},\boldsymbol{\nu})W(\boldsymbol{\nu}), \tag{A.12a}$$

$$p_{011}(\boldsymbol{\mu},\boldsymbol{\nu}) = 1. \tag{A.12b}$$

Comparing to the consistency requirements (A.5) we see that it always satisfies (A.5b), but only satisfies (A.5a) if

$$\frac{1}{W(\boldsymbol{\mu}+\boldsymbol{\nu})} = \frac{1}{W(\boldsymbol{\mu})} + \frac{1}{W(\boldsymbol{\nu})}. \tag{A.13}$$

If we assume that W is continuous, (A.13) implies that $1/W$ is linear. So, for example, assuming that $W(\boldsymbol{\mu}) = W(\mu)$, i.e. that W depends only on the total mass, then

$$W(\boldsymbol{\mu}) \propto \mu^{-1}$$

corresponding to mass-weighted (or volume-weighted) schemes. More generally, it must be true that

$$W(\boldsymbol{\mu}) = \frac{1}{\sum_{a=1}^{A}\beta_a\mu_a}$$

for some set of real weights $\{\beta_a\}_{a=1}^{A}$. If we symmetrize this method as described above, i.e. choose

$$R(\boldsymbol{\mu},\boldsymbol{\nu}) = (W(\boldsymbol{\mu}) + W(\boldsymbol{\nu}))K(\boldsymbol{\mu},\boldsymbol{\nu}), \tag{A.14a}$$

$$\tilde{p}_{011}(\boldsymbol{\mu},\boldsymbol{\nu}) = \frac{W(\boldsymbol{\nu})}{W(\boldsymbol{\mu}) + W(\boldsymbol{\nu})}, \tag{A.14b}$$

$$\tilde{p}_{101}(\boldsymbol{\mu},\boldsymbol{\nu}) = \frac{W(\boldsymbol{\mu})}{W(\boldsymbol{\mu}) + W(\boldsymbol{\nu})}, \tag{A.14c}$$

which for $W(\boldsymbol{\mu}) = 1/\mu$ are:

$$R(\boldsymbol{\mu},\boldsymbol{\nu}) = \left(\frac{1}{\mu} + \frac{1}{\nu}\right)K(\boldsymbol{\mu},\boldsymbol{\nu}), \tag{A.15a}$$

$$\tilde{p}_{011}(\boldsymbol{\mu},\boldsymbol{\nu}) = \frac{\mu}{\mu+\nu}, \tag{A.15b}$$

$$\tilde{p}_{101}(\boldsymbol{\mu},\boldsymbol{\nu}) = \frac{\nu}{\mu+\nu}, \tag{A.15c}$$

Table A.2
List of symbols.

Symbol	Definition
α	Weighting exponent, see (4)
$c(\boldsymbol{\mu},t)$	Computational number concentration, see (7)
$c_{\text{emit}}(\boldsymbol{\mu},t)$	Aerosol number distribution of emitted computational particles, see (31)
$\text{CV}(X)$	Sample coefficient of variation of random variable X, see (46)
$D(\boldsymbol{\mu})$	Diameter of particle with constituent masses $\boldsymbol{\mu}$, see (4)
D_{gn}	Geometric mean diameter of a log-normal distribution, see (34)
$\delta(\boldsymbol{\mu})$	Dirac delta function
$\boldsymbol{g}(t)$	Vector of gas phase species concentrations, see (2)
$\boldsymbol{g}_{\text{back}}(t)$	Background gas concentrations, see (2)
$\dot{\boldsymbol{g}}_{\text{emit}}(t)$	Gas emission rate, see (2)
γ_α	Weighting factor, see (51)
$\boldsymbol{I}(\boldsymbol{\mu},\boldsymbol{g},t)$	Gas-to-particle flux-rate vector, see (2)
$I^w(\boldsymbol{\mu},\boldsymbol{g},t)$	Water-particle flux rate, see (2)
$K(\boldsymbol{\mu},\boldsymbol{\nu})$	Coagulation kernel for particles with masses $\boldsymbol{\mu}$ and $\boldsymbol{\nu}$, see (2)
κ	Hygroscopicity parameter
$\lambda_{\text{dil}}(t)$	Dilution rate with background, see (2)
$m(D)$	Aerosol mass distribution at diameter D, see (41)
$M(t)$	Total aerosol mass concentration
$\boldsymbol{\mu}$	Vector of particle constituent masses
μ^a	Mass of species a
$n(D)$	Aerosol number distribution at diameter D, see (40)
$n(\boldsymbol{\mu},t)$	Aerosol number distribution at time t and constituent masses $\boldsymbol{\mu}$, see (2)
$n_{\text{back}}(\boldsymbol{\mu},t)$	Aerosol number distribution of background particles, see (2)
$\dot{n}_{\text{emit}}(\boldsymbol{\mu},t)$	Aerosol number distribution of particle emission rate, see (2)
$N(\boldsymbol{\mu},t)$	Cumulative aerosol number distribution at time t and constituent masses $\boldsymbol{\mu}$
$N(t)$	Total number concentration
N_{p}	Number of computational particles, see (3)
$p(t)$	Air pressure, see (2)
Π	Finite sample of aerosol particles, see Section 3
$\boldsymbol{R}(\boldsymbol{g})$	Gas concentration growth rate due to gas chemical reactions, see (2)
$\boldsymbol{R}(\boldsymbol{\mu},\boldsymbol{\nu})$	Weighted coagulation kernel, see (12a)
R	Number of realizations, see Section 6.2
$\text{RH}(t)$	Relative humidity
$\rho_{\text{dry}}(t)$	Dry air density, see (2)
S_{c}	Critical supersaturation
S_{env}	Threshold for environmental supersaturation
$\sigma(X)$	Sample standard deviation of random variable X, see (45)
σ_{g}	Geometric standard deviation of a log-normal distribution, see (34)
$T(t)$	Temperature
V	Computational volume, see (3)
w_{BC}	Black carbon mass fraction
$W(\boldsymbol{\mu})$	Weighting function, see (4)
$\overline{x(t)}$	Time average of quantity x, see (47)
$\langle X\rangle$	Sample mean of random variable X, see (44)

then we see that (A.15) satisfies (A.8), so MFA is optimal. Note that MFA and our $\alpha = 3$ scheme are similar but not the same, but if we make a simple modification to MFA; namely, choosing

$$R(\boldsymbol{\mu}, \boldsymbol{v}) = \left(\frac{1}{\mu} + \frac{1}{v}\right) K(\boldsymbol{\mu}, \boldsymbol{v}), \tag{A.16a}$$

$$p_{\text{birth}}(\boldsymbol{\mu}, \boldsymbol{v}) = \frac{v}{\mu + v}, \tag{A.16b}$$

$$p_{\text{death}}(\boldsymbol{\mu}, \boldsymbol{v}) = 1 \tag{A.16c}$$

in an independent scheme as described in the body of the paper, then this recovers (15).

References

[1] M.J. Cubison, B. Ervens, G. Feingold, K.S. Docherty, I.M. Ulbrich, L. Shields, K. Prather, S. Hering, J.L. Jimenez, The influence of chemical composition and mixing state on Los Angeles urban aerosol on CCN number and cloud properties, Atmos. Chem. Phys. 8 (2008) 5629–5681.
[2] R.A. Zaveri, R.C. Easter, J.D. Fast, L.K. Peters, Model for simulating aerosol interactions and chemistry (MOSAIC), J. Geophys. Res. 113 (2008) D13204.
[3] A.S. Wexler, F.W. Lurmann, J.H. Seinfeld, Modelling urban aerosols-I. Model development, Atmos. Environ. 28 (1994) 531–546.
[4] M.J. Kleeman, G.R. Cass, A 3D Eulerian source-oriented model for an externally mixed aerosol, Environ. Sci. Technol. 35 (2001) 4834–4848.
[5] M.Z. Jacobson, Analysis of aerosol interactions with numerical techniques for solving coagulation, nucleation, condensation, dissolution, and reversible chemistry among multiple size distributions, J. Geophys. Res. 107 (2002) 4366.
[6] P.J. Adams, J.H. Seinfeld, D.M. Koch, Global concentration of tropospheric sulphate, nitrate and ammonium simulated in a general circulation model, J. Geophys. Res. 104 (1999) 13791–13823.
[7] J. Wilson, C. Cuvelier, F. Raes, A modeling study of global mixed aerosol fields, J. Geophys. Res. 106 (2001) 34081–34108.
[8] P. Stier, J. Feichter, S. Kinne, S. Kloster, E. Vignati, J. Wilson, L. Ganzeveld, I. Tegen, M. Werner, Y. Balkanski, M. Schulz, O. Boucher, A. Minikin, A. Petzold, The aerosol-climate model ECHAM5-HAM, Atmos. Chem. Phys. 5 (2005) 1125–1156.
[9] F.S. Binkowski, U. Shankar, The regional particulate matter model, 1. Model description and preliminary results, J. Geophys. Res. 100 (1995) 26191–26209.
[10] N. Riemer, H. Vogel, B. Vogel, F. Fiedler, Modeling aerosols on the mesoscale γ, part I: Treatment of soot aerosol and its radiative effects, J. Geophys. Res. 108 (2003) 4601.
[11] R. Zaveri, J. Barnard, R. Easter, N. Riemer, M. West, Effect of aerosol mixing-state on optical and cloud activation properties, J. Geophys. Res 115 (2010) D17210.
[12] Y. Efendiev, M.R. Zachariah, Hybrid Monte Carlo method for simulation of two-component aerosol coagulation and phase segregation, J. Colloid Interf. Sci. 249 (2002) 30–43.
[13] A. Maisels, F.E. Kruis, H. Fissan, Direct simulation Monte Carlo for simultaneous nucleation, coagulation, and surface growth in dispersed systems, Chem. Eng. Sci. 59 (2004) 2231–2239.
[14] N. Riemer, M. West, R. Zaveri, R. Easter, Simulating the evolution of soot mixing state with a particle-resolved aerosol model, J. Geophys. Res. (2009).
[15] D.T. Gillespie, An exact method for numerically simulating the stochastic coalescence process in a cloud, J. Atmos. Sci. 32 (1975) 1977–1989.
[16] D.T. Gillespie, A general method for numerically simulating the stochastic time evolution of coupled chemical reactions, J. Comput. Phys. 22 (1976) 403–434.
[17] D.T. Gillespie, Exact stochastic simulation of coupled chemical reactions, J. Phys. Chem. 81 (1977) 2340–2361.
[18] D.T. Gillespie, Markov Processes: An Introduction for Physical Scientists, Academic Press, 1992.
[19] S. Shima, K. Kusano, A. Kawano, T. Sugiyama, S. Kawahara, The super-droplet method for the numerical simulation of clouds and precipitation: a particle-based and probabilistic microphysics model coupled with a non-hydrostatic model, Q. J. R. Meteorol. Soc. 135 (2009) 1307–1320.
[20] H. Babovsky, On a Monte Carlo scheme for Smoluchowski's coagulation equation, Monte Carlo Methods Appl. 5 (1999) 1–18.
[21] A. Eibeck, W. Wagner, Stochastic particle approximations for Smoluchowski's coagulation equation, Preprint 585, Weierstrass-Institut for Applied Analysis and Stochastics, 2000.
[22] A. Eibeck, W. Wagner, An efficient stochastic algorithm for studying coagulation dynamics and gelation phenomena, SIAM J. Sci. Comput. 22 (2000) 802–821.
[23] A. Eibeck, W. Wagner, Approximative solution of the coagulation-fragmentation equation by stochastic particle systems, Stoch. Anal. Appl. 18 (2000) 921–948.
[24] A. Eibeck, W. Wagner, Stochastic particle approximations for Smoluchoski's coagulation equation, Ann. Appl. Probab. 11 (2001) 1137–1165.
[25] A. Eibeck, W. Wagner, Stochastic interacting particle systems and nonlinear kinetic equations, Ann. Appl. Probab. 13 (2003) 845–889.
[26] A. Kolodko, K. Sabelfeld, Stochastic particle methods for Smoluchowski coagulation equation: variance reduction and error estimations, Monte Carlo Methods Appl. 9 (2003) 315–339.
[27] R. Irizarry, Fast Monte Carlo methodology for multivariate particulate systems—I: Point ensemble Monte Carlo, Chem. Eng. Sci. 63 (2008) 95–110.
[28] R. Irizarry, Fast Monte Carlo methodology for multivariate particulate systems—II: τ-PEMC, Chem. Eng. Sci. 63 (2008) 111–121.
[29] C.G. Wells, M. Kraft, Direct simulation and mass flow stochastic algorithms to solve a sintering-coagulation equation, Monte Carlo Methods Appl. 11 (2005) 175–197.
[30] H. Zhao, C. Zheng, M. Xu, MultiMonte Carlo Method for coagulation and condensation/evaporation in dispersed systems, J. Colloid Interface Sci. 286 (2005) 195–208.
[31] H. Zhao, C. Zheng, Correcting the MultiMonte Carlo Method for particle coagulation, Powder Technol. 193 (2009) 120–123.
[32] H. Zhao, F. Kruis, C. Zheng, Reducing statistical noise and extending the size spectrum by applying weighted simulation particles in Monte Carlo simulation of coagulation, Aerosol Sci. Technol. 43 (2009) 781–793.
[33] E. Debry, B. Sportisse, B. Jourdain, A stochastic approach for the numerical simulation of the general dynamics equations for aerosols, J. Comput. Phys. 184 (2003) 649–669.
[34] N. Morgan, C. Wells, M. Kraft, W. Wagner, Modelling nanoparticle dynamics: coagulation, sintering, particle inception and surface growth, Combust. Theory Model. 9 (2005) 449–461.
[35] N.M. Morgan, C.G. Wells, M.J. Goodson, M. Kraft, W. Wagner, A new numerical approach for the simulation of the growth of inorganic nanoparticles, J. Comput. Phys. 211 (2006) 638–658.
[36] R.I.A. Patterson, M. Kraft, Weighted particle methods for the Smoluchowski coagulation equation, Technical Report ISSN 1473-4273, Cambridge Centre for Computational Chemical Engineering, Department of Chemical Engineering, University of Cambridge, Cambridge, CB2 3RA, United Kingdom, 2007.
[37] M. Celnik, R. Patterson, M. Kraft, W. Wagner, Coupling a stochastic soot population balance to gas-phase chemistry using operator splitting, Combust. Flame 148 (2007) 158–176.
[38] M. Celnik, R. Patterson, M. Kraft, W. Wagner, A predictor-corrector algorithm for the coupling of stiff ODEs to a particle population balance, J. Comput. Phys. 228 (2009) 2758–2769.

[39] H. Zhao, C. Zheng, A new event-driven constant-volume method for solution of the time evolution of particle size distribution, J. Comput. Phys. 228 (2009) 1412–1428.
[40] D.E. Knuth, The Art of Computer Programming, Seminumerical Algorithms, third ed., vol. 2, Addison Wesley, 1998.
[41] A. Shwartz, A. Weiss, Large Deviations for Performance Analysis, Chapman & Hall, London, 1995.
[42] J. Norris, Smoluchowski's coagulation equation: uniqueness, nonuniqueness and a hydrodynamic limit for the stochastic coalescent, Ann. Appl. Prob. 9 (1999) 78–109.
[43] R.E.L. DeVille, N. Riemer, M. West, Convergence of a generalized Weighted Flow Algorithm (WFA) for stochastic particle coagulation, in preparation.
[44] D.T. Gillespie, Stochastic simulation of chemical kinetics, Ann. Rev. Phys. Chem. 58 (2007) 35–55.
[45] D.T. Gillespie, Approximate accelerated stochastic simulation of chemically reacting systems, J. Chem. Phys. 115 (2001) 1716–1733.
[46] M.Z. Jacobson, Isolation nitrated and aromatic aerosols and nitrated aromatic gases as sources of ultraviolet light absorption, J. Geophys. Res. 104 (1999) 3527–3542.
[47] A. Bott, A flux method for the numerical solution of the stochastic collection equation, J. Atmos. Sci. 55 (1998) 2284–2293.
[48] R.A. Zaveri, L.K. Peters, A new lumped structure photochemical mechanism for large-scale applications, J. Geophys. Res. 104 (1999) 30387–30415.
[49] R.A. Zaveri, R.C. Easter, A.S. Wexler, A new method for multicomponent activity coefficients of electrolytes in aqueous atmospheric aerosols, J. Geophys. Res. 110 (2005) D02210, doi:10.1029/2004JD004681.
[50] R.A. Zaveri, R.C. Easter, L.K. Peters, A computationally efficient multicompoennt equilibrium solver for aerosols (MESA), J. Geophys. Res. 110 (2005) D24203.
[51] D. Delene, J. Ogren, Variability of aerosol optical properties at four North American surface monitoring sites, J. Atmos. Sci. 59 (2002) 1135–1150.
[52] A. Dubovik, B. Holben, T.F. Eck, A. Smirnov, Y. Kaufman, M.D. King, D. Tanre, I. Slutsker, Variability of absorption and optical properties of key aerosol types observed in worldwide locations, J. Atmos. Sci. 59 (2002) 590–608.
[53] N. Riemer, M. West, R. Zaveri, R. Easter, Estimating black carbon aging time-scales with a particle-resolved aerosol model, J. Aerosol Sci. 41 (2010) 143–158.